

Ice-Nucleating Particles Near Two Major Dust Source Regions

Charlotte M. Beall^{1,2}, Thomas C. J. Hill³, Paul J. DeMott³, Tobias Köneman^{2*}, Michael Pikridas⁴,
Frank Drewnick⁵, Hartwig Harder⁶, Christopher Pöhlker², Jos Lelieveld^{4,6}, Bettina Weber^{2**},
Minas Iakovides⁴, Roman Prokeš^{7,8}, Jean Sciare⁴, Meinrat O. Andreae^{1,2,9}, M. Dale Stokes¹,
Kimberly A. Prather^{1,10}

¹Scripps Institution of Oceanography, University of California San Diego, La Jolla, CA 92037, USA

²Max Planck Institute for Chemistry, Multiphase Chemistry and Biogeochemistry Departments, D-55128 Mainz, Germany

³Department of Atmospheric Science, Colorado State University, Fort Collins, CO 80523, USA

⁴Climate & Atmosphere Research Center, The Cyprus Institute, Nicosia, CY-1645, Cyprus

⁵Max Planck Institute for Chemistry, Particle Chemistry Department, D-55128 Mainz, Germany

⁶Max Planck Institute for Chemistry, Atmospheric Chemistry Department, D-55128 Mainz, Germany

⁷RECETOX, Faculty of Science, Masaryk University, Kotlarska 2, 611 Brno, Czech Republic

⁸Department of Atmospheric Matter Fluxes and Long-range Transport, Global Change Research Institute of the Czech Academy of Sciences, Belidla 4a, 60300, Brno, Czech Republic

⁹Department of Geology and Geophysics, King Saud University, Riyadh, Saudi Arabia

¹⁰Department of Chemistry and Biochemistry, University of California San Diego, La Jolla, CA, 92093 USA

*Now at Envicontrol GmbH, Waidmarkt 11, 50676 Köln, Germany

**Now at: Institute of Biology, University of Graz, 8010 Graz, Austria

32 Correspondence to: Charlotte M. Beall, cbeall@ucsd.edu

33 Abstract

34 Mineral dust and sea spray aerosol represent important sources of ice-nucleating particles (INPs), the minor
35 fraction of aerosol particles able to trigger cloud ice crystal formation and, consequently, influence multiple
36 climate-relevant cloud properties including lifetime, radiative properties and precipitation initiation
37 efficiency. Mineral dust is considered the dominant INP source in many parts of the world due to its ice
38 nucleation efficiency and its sheer abundance, with global emission rates of up to 4700 Tg a⁻¹. However,
39 INPs emitted from the ocean surface in sea spray aerosol frequently dominate INP populations in remote
40 marine environments, including parts of the Southern Ocean where cloud-resolving model simulations have
41 demonstrated that cloud radiative properties are likely strongly controlled by INPs. Here we report INP
42 concentrations measured in aerosol and seawater samples during Air Quality and Climate Change in the
43 Arabian BASin (AQABA), a shipborne campaign that spanned the Red Sea, Gulf of Aden, Arabian Sea,
44 Arabian Gulf, and part of the Mediterranean. In aerosol samples collected within a few hundred kilometers
45 of the first and second ranked sources of dust globally, the Sahara and Arabian Peninsula, INP
46 concentrations ranged from 0.2 to 11 L⁻¹ at -20 °C with observed ice-active surface site densities (n_s) 1-3
47 orders of magnitude below levels predicted by mineral dust INP parameterizations. Over half of the samples
48 (at least 14 of 26) were collected during dust storms with average dust mass concentrations between 150
49 and 490 µg m⁻³ (PM₁₀), as simulated by the Modern-Era Retrospective analysis for Research and
50 Application, version 2 (MERRA-2). The impacts of heat and peroxide treatments indicate that organics
51 dominated the observed ice nucleation (IN) -activity at temperatures ≥ -15 °C with proteinaceous (heat-
52 labile) INPs frequently observed at high freezing temperatures > -10 °C. INP concentrations in seawater
53 samples ranged between 3 and 46 mL⁻¹ at -19 °C, demonstrating the relatively low INP source potential of
54 seawater in the region as compared to seawater from multiple other regions reported previously. Overall,
55 our results demonstrate that despite proximity to the Sahara and the Arabian Peninsula and the dominance
56 of mineral dust in the aerosol sampled, existing mineral dust parameterizations alone would not skillfully
57 represent the near-surface n_s in the observed temperature regime (-6 to -25 °C). Future efforts to develop
58 or improve representations of dust INPs at modest supercooling (≥ -15 °C) would benefit from a
59 characterization of the specific organic species associated with dust INPs. More generally, an improved
60 understanding of the organic species associated with increased IN -activity and their variability across dust
61 source regions would directly inform efforts to determine whether n_s -based parameterizations are
62 appropriate for faithful representation of dust INPs in this sensitive temperature regime, whether region-
63 specific parameterizations are required, or whether an alternative to the n_s approach is necessary.

64 **1 Introduction**

65 Ice-nucleating particles (INPs) modulate the temperature and relative humidity at which ice
66 particle formation occurs in the atmosphere and thus are a key factor that controls ice-phase
67 partitioning in clouds. As initiators of ice formation and related phase-partitioning processes, INPs
68 affect multiple cloud properties and exert a strong influence on cloud lifetime, radiative properties
69 and precipitation initiation efficiency (e.g. Lohmann and Feichter, 2005; Vergara-Temprado et al.,
70 2018; Brunner et al., 2021).

71 Globally, desert dust is likely the most abundant aerosol type by mass (Kinne et al., 2006; Kok et
72 al., 2021). Furthermore, multiple studies have demonstrated that mineral dust is the dominant ice-
73 nucleating species in many parts of the world based on observations (Ardon-Dryer and Levin,
74 2014; Boose et al., 2016; DeMott et al., 2015a; Price et al., 2018) and modeling of global INP
75 distributions (Burrows et al., 2013; Hoose et al., 2010; Murray et al., 2012; Vergara-Temprado et
76 al., 2017). Annual global dust emission rate estimates range between 400 and 4700 Tg a⁻¹ (Huneeus
77 et al., 2011; Kok et al., 2021). Of the average global dust loading in the atmosphere (20-29 Tg),
78 North African source regions are estimated to contribute ~50% (11-15 Tg), and the Middle East
79 and Central Asian source regions account for the bulk of the remainder, ~30% (7.7 Tg) (Kok et
80 al., 2021). Analysis of satellite products indicates that dust emission rates are increasing over the
81 Middle East at a rate of 15% a⁻¹ (Klingmüller et al., 2016; Yu et al., 2018).

82 While Hoose and Möhler (2012) showed that mineral dust INPs generally activate ice crystals at
83 freezing temperatures < -15 °C, dust containing K-feldspar has been shown to nucleate ice at much
84 warmer temperatures, up to -4 °C (Atkinson et al., 2013; Harrison et al., 2016; Niedermeier et al.,
85 2015; Wex et al., 2014; Whale et al., 2015; Zolles et al., 2015). K-feldspars represent up to ~24%
86 of Saharan and Asian dusts by mass (Nickovic et al., 2012). However, knowledge of the abundance
87 and the available surface fraction of aerosolized K-feldspar would be necessary to evaluate the IN
88 efficiency of dust at temperatures > -15 °C (Kanji et al., 2017).

89 Though mineral dust is considered to be the dominant INP source in many regions, multiple
90 modeling and observational studies suggest that marine INPs are frequently dominant by number
91 in remote ocean regions in air masses with low concentrations of terrestrial aerosol (McCluskey et
92 al., 2018b, 2018c; Vergara-Temprado et al., 2017; Wilson et al., 2015; DeMott et al., 2016). Using

93 a global aerosol model to simulate marine organic and K-feldspar INP populations, Vergara-
94 Temprado et al. (2017) showed that the relative contribution of marine organic vs. dust INPs in
95 remote regions varies seasonally, and that marine organic INPs frequently outnumber K-feldspar
96 INPs (up to 100% of the simulated days in the Southern Ocean during summer). Results from a
97 follow-on cloud-resolving model study showed that Southern Ocean cloud reflectivity is strongly
98 modulated by INP concentrations, indicating that accurate estimates of the radiative energy budget
99 in the Southern Ocean likely require improved and reliable representation of both dust and marine
100 organic INPs (Vergara-Temprado et al., 2018). By generating isolated nascent sea spray aerosol
101 over a range of biological conditions, mesocosm studies have shown that marine INPs are
102 comprised of two classes: a dissolved organic carbon (DOC) type composed of IN-active
103 molecules and a particulate organic carbon (POC) type linked to the death phase of phytoplankton
104 blooms (McCluskey et al., 2017, 2018b).

105 Parameterizations for both marine and mineral dust populations are commonly implemented in
106 atmospheric models to estimate dust and marine INP concentrations. There are multiple existing
107 mineral dust INP parameterizations used to estimate their concentrations in aerosolized desert dust,
108 some based exclusively on laboratory measurements (e.g., Niemand et al., 2012; Ullrich et al.,
109 2017), and others derived from a combination of laboratory and field measurements (DeMott et
110 al., 2015). There are, additionally, multiple mineral-specific INP parameterizations including illite
111 (Broadley et al., 2012), kaolinite (Welti et al., 2012), quartz (Harrison et al., 2019) and K-feldspar
112 (Atkinson et al., 2013; hereafter, "A13"). The parameterizations by Ullrich et al. (2017; hereafter,
113 "U17") and Niemand et al. (2012; hereafter, "N12") were developed using dust samples from
114 multiple deserts, and both found little variability in the IN activity between dusts from locations
115 as disparate as the Sahara and Asia. DeMott et al. (2015; hereafter, "D15") found agreement
116 between their observations-based parameterization and N12, supporting the validity of laboratory-
117 based parameterizations. Results in D15 also confirmed the conclusions of N12 and U17: that to
118 first order, dusts from distinct regions can be parameterized as a single particle type. The D15
119 parameterization has been considered to be representative of dust that has undergone atmospheric
120 photochemical and oxidative processes in transport (i.e., "aged" dust), because the
121 parameterization was derived from observations made far (1000s of kilometers) from the dust
122 emissions sources (Boose et al., 2016).

123 By contrast, few studies report *in situ* INP measurements near (e.g., < 1 day of transport) a major
124 dust source, and the lack of observations near dust source regions inhibit the evaluation of the
125 ability of existing dust INP parameterizations to represent nascent dust populations (Boose et al.,
126 2016; Gong et al., 2020; Price et al., 2018). INP observations are particularly lacking for the
127 sensitive temperature regime > -20 °C. Boose et al. (2016) found that D15 overpredicted INPs
128 observed during Saharan dust events at a location within 100s of km west of the Sahara (Izaña,
129 Tenerife, Spain) by 2-3 orders of magnitude, suggesting that aging may lead to increased IN
130 efficiency in mineral dust and that D15 may be less representative of nascent dust. These
131 conclusions were supported by Conen et al. (2015), who found that concentrations of INPs at -20
132 °C measured during Saharan dust events were one order of magnitude higher at Jungfrauoch in
133 the Swiss Alps than in Izaña, where dust events had occurred 1-7 d prior to reaching Jungfrauoch.
134 Gong et al. (2020) measured INPs in a variety of atmospheric and seawater sample types at Cabo
135 Verde and determined mineral dust to be the dominant source of INPs observed in the atmosphere
136 but found that INPs with freezing temperatures > -10 °C were likely biological. At altitudes
137 between 30 and 3500 m in the same region, Price et al. (2018) found that measured concentrations
138 of INPs ranged two orders of magnitude at a given temperature, and that the observed
139 concentrations related to the atmospheric dust loadings.

140 Recently, multiple studies have provided new, much-needed observations of ambient atmospheric
141 INPs in marine environments (DeMott et al., 2016; Hartmann et al., 2020; McCluskey et al., 2018c,
142 2018d; Yang et al., 2020) where data was historically lacking and, consequently, an impediment
143 to achieving predictive understanding of global INP distributions (Burrows et al., 2013). There
144 are now two parameterizations available for the estimation of atmospheric concentrations of
145 marine INPs emitted from the ocean surface: Wilson et al. (2015), which estimates cumulative
146 INPs from total organic carbon (TOC) concentrations in simulated sea spray aerosol (SSA), and
147 McCluskey et al. (2018), which estimates ice-active surfacesite density (n_s) from aerosol surface
148 area. Wilson et al. (2015) and McCluskey et al. (2018; hereafter “M18”) derived marine INP
149 parameterizations from field measurements of INPs in Atlantic and Arctic Ocean sea surface
150 microlayer samples and pristine SSA samples over the North Atlantic Ocean, respectively.

151 Here, we report observations of INPs measured in air masses influenced by both desert dust and
152 marine aerosol (Edtbauer et al., 2020) in close proximity to the two greatest global dust aerosol

153 sources: the Sahara (#1) and the Arabian Peninsula (#2) (Kok et al., 2021). INP concentrations
154 were measured in 26 ambient aerosol samples collected during Air Quality and Climate Change
155 in the Arabian Basin (AQABA), a shipborne campaign which took place July – August 2017 on a
156 transect that spanned the central and eastern parts of the Mediterranean, the Red Sea, the Gulf of
157 Aden, the Arabian Sea and the Arabian Gulf. The rest of this study will be structured as follows.
158 We present an overview of measurements and data sources in Sect. 2 Methods. In Results Sect.
159 3.1, an overview of INP concentrations observed is presented, followed by an assessment of
160 subsurface seawater (SSW) source potential (Sect. 3.2). Observed n_s are compared to dust and
161 marine INP parameterizations in Sect. 3.3, followed by an analysis of the contributions of heat-
162 labile (e.g., proteinaceous) and heat-stable organic compounds to observed INP populations in
163 aerosol (Sect. 3.4). The same analysis is applied to assess organic contributions to observed INPs
164 in a soil dust sample from a likely source region in Sect. 3.5. We discuss the findings, potential
165 INP sources and compare with prior studies in the Discussion Sect. 5. Finally, in Sect. 5 we offer
166 strategies to address the challenges of evaluating dust-specific INP parameterizations and
167 recommend measurements needed to develop predictive understanding of dust INPs at modest
168 supercooling ($T \geq 15^\circ\text{C}$).

169 **2 Methods**

170 **2.1 Project Overview**

171 The AQABA campaign was conducted from 25 June to 3 September 2017 onboard the RV
172 *Kommandor Iona*. The research voyage was conducted in two transects: the first leg beginning in
173 La-Seyne-sur-Mer, France, heading through the Suez Canal, around the Arabian Peninsula and
174 ending in Kuwait, and second leg a return transect via the same route (Figs. S1-S2). The campaign
175 supported a large suite of on- and offline aerosol and gas-phase measurements (Bourtsoukidis et
176 al., 2019, 2020; Celik et al., 2020; Edtbauer et al., 2020; Eger et al., 2019; Friedrich et al., 2021;
177 Pfannerstill et al., 2019; Tadic et al., 2020; Wang et al., 2020).

178 **2.2 Aerosol and Trace Gas Measurements**

179 Aerosol size distributions were measured using an Optical Particle Spectrometer (OPC, Grimm
180 model 1.109) and a Fast Mobility Particle Spectrometer (FMPS, TSI model 3091). The OPC

181 measures particles in the size range 0.25 – 32 μm , and the FMPS measures particles with sizes
182 between 5.6 nm and 560 nm with 6s and 1s time resolution, respectively. The inlet for the aerosol
183 instrumentation was located at the top of a measurement container at a horizontal distance of about
184 15 m from the INP filter sampling unit (Figs. S3-S4). To avoid condensation in inlet lines, aerosol
185 samples were passed through a drying system, which reduced ambient relative humidity (RH) to
186 an average value of $\approx 40\%$ in the measurement container. Ambient RH ranged between 67 and
187 81% during INP sampling periods. OPC and FMPS data were averaged over 1-minute time
188 intervals. A filter flag based on aerosol measurements was derived to identify and eliminate stack
189 emissions and applied to all aerosol data. The filter flag was based on short term variation in
190 particle number concentration measured by a Condensation Particle Counter (CPC, TSI model
191 3787), black carbon concentrations (Aethalometer, Magee AE33), wind direction and speed. The
192 flag was set when the apparent wind direction was from the direction of the stack ($\pm 30^\circ$) as seen
193 from the aerosol inlet position (Fig. S3) and strong fluctuations of black carbon and/or particle
194 number concentrations were observed relative to background levels. Particle losses were estimated
195 using the Particle Loss Calculator (von der Weiden et al., 2009). Losses were negligible ($<1\%$) up
196 to 3.5 μm and increased to 40% at 10 μm .

197 Particle surface area concentrations were derived from the 1-min time-averaged FMPS and OPC
198 measurements as follows. Geometric diameters were estimated from the measured mobility
199 diameters (FMPS) and optical particle diameters (OPC). Aerosols were assumed dry at sampling
200 conditions following the drying system described above. To convert optical particle diameters into
201 geometric diameters, it was assumed that all coarse particles ($d_p > 3000\text{ nm}$) were composed of
202 sea salt and dust with a mass ratio of 25% to 75%, and using the respective refractive indices and
203 shapes the measured optical particle diameters were converted into geometric diameters (Sect.
204 S1.1). The sea salt:dust mass ratio was based on average dust and sea salt concentrations as
205 measured in particles $< 10\ \mu\text{m}$ (PM_{10} ; see Sect. S2 for details).

206 Fine particle ($d_p < 700\text{ nm}$) size was converted from optical diameter (d_{opt}) into geometric diameter
207 (d_{geo}) using the optical properties calculated from the chemical composition of particles $< 1\ \mu\text{m}$
208 (PM_1) as measured by an Aerosol Mass Spectrometer (Aerodyne HR-ToF-AMS), assuming
209 spherical particles. For particles in the intermediate size range (700 – 3000 nm), log-linear
210 interpolation of optical and spherical properties was applied for conversion of optical into

211 geometric particle diameters (Sect. S1.2). The mobility diameters measured by the FMPS were
212 considered equivalent to the geometric diameter, assuming spherical particles. From the resulting
213 particle size distributions, particle surface area was calculated for each size bin. Total particle
214 surface concentrations were determined by integrating the surface area distribution for particles up
215 to 10 μm (d_{geo}). The overall uncertainty of derived particle surface area concentrations is estimated
216 to be 30%, including the uncertainty due to particle losses (see Sect. S3).

217 The water-soluble fraction of total suspended particles (TSPs) was monitored with hourly
218 resolution using a Monitor for AeRosols and Gases in Ambient Air, MARGA (Metrohm Applikon
219 model S2, Herisau, Switzerland). Sea salt concentrations were estimated by scaling measured
220 soluble Na^+ concentrations by 3.27 following Manders et al. (2009) and were used as a proxy for
221 SSA number concentrations. Size-resolved single particle chemical composition measurements
222 have shown that sea salt represents 50-70% of SSA particles by number ($d_p > 0.5\mu\text{m}$) (Collins et
223 al., 2014) Hourly composition data was linearly interpolated for 4 samples where 1-3 hours (of 7-
224 24 hours total sampling time) was missing (Fig. S5). The MARGA sampling line was
225 equipped with a PM_{10} cyclone, but the sample was not dried as the instrument is not prone to
226 condensation. Particle transmission losses to the MARGA were estimated using the PLC and found
227 to be consistent with the aerosol sizing instruments described above.

228 Nitric oxide (NO) concentrations were measured using a commercially available two-channel
229 chemiluminescence monitor, CLD 790 SR (ECO Physics AG, Dürnten, Switzerland). During the
230 AQABA campaign, the CLD 790 SR, MARGA, FMPS, OPC, HR-ToF-AMS, CPC and
231 Aethalometer were operated within laboratory containers on the main deck of the research vessel.
232 The NO measurements were used to prevent stack sampling during INP collection (see Sect. 2.4).

233 **2.3 Dust Mass Concentrations from MERRA-2**

234 Since dust concentrations were not measured during the campaign, hourly dust surface mass
235 concentrations along the cruise track were obtained from the ($0.5 \times 0.625^\circ$) Modern-Era
236 Retrospective analysis for Research and Application, version 2 (MERRA-2; Gelaro et al., 2017)
237 and were averaged over the region covered during each sampling period. Buchard et al. (2017)
238 showed a high degree of correlation between MERRA-2 and surface dust concentration
239 observations ($r \geq 0.69$), particularly during dust storms ($r \geq 0.92$). MERRA-2 surface dust mass

240 concentrations also correlated well with PM_{10} observed during AQABA ($r \geq 0.71$) (Fig. S6).
241 MERRA-2 uses the GEOS-5 Earth system model (Molod et al., 2015; Rienecker et al., 2011) with
242 72 vertical layers between the surface and 0.01 hPa (~ 80 km) and the three-dimensional variational
243 data assimilation Gridpoint Statistical Interpolation analysis system (Kleist et al., 2009; Wu et al.,
244 2002, additional details in Sect. S4).

245 **2.4 INP Measurements in Aerosol**

246 Ambient aerosol sampling for offline measurement of INPs was conducted from 5 Jul – 31 Aug
247 2017 on the *Kommandor Iona's* wheelhouse top (platform above the bridge), ~ 15 m horizontally
248 from the online aerosol measurements inlet and ~ 15 m from the ocean surface (Figs. S3-4).
249 Sampling locations along the cruise transect corresponding to each aerosol sample are shown in
250 Figs. S1-2.

251 Aerosol samples were collected over 3-28 hour periods on polycarbonate filters (47 mm diameter,
252 $0.2 \mu\text{m}$ pore-size, Whatman® Nuclepore, Chicago, Illinois, USA) placed in open-face Nalgene®
253 Analytical Filter Units (Waltham, Massachusetts, USA). Sampling intervals and frequency were
254 chosen with the aim of collecting > 5000 L during dust events and $> 10,000$ L when OPC particle
255 counts were relatively low (e.g., during sampling periods f040-44), as conditions allowed. Aerosol
256 sampling flow rates through the filter units were set to 10-13 LPM using a MassStream™ mass
257 flow controller (Bethlehem, PA, USA) connected inline with a rotary vane pump (Thomas QR-
258 0100, Gardner Denver ©, Monroe, LA, USA). To decrease exposure to stack emissions, the pump
259 was automated to switch off when online measurements of NO exceeded one standard deviation
260 above the average background concentration for over 1 minute ($\sim 0.4 \pm 0.8$ ppb). Comparing the
261 stack contamination filter flag for aerosol measurements (Sect. 2.2) with INP sampling periods
262 additionally indicates no influence of stack emissions on INP filter samples. Lacking a size-
263 selective inlet for INP sampling, it is possible that aerosols $> 10 \mu\text{m}$ were present in INP samples
264 during dust events. Surface area may be underestimated for these samples due to the PM_{10} cutoff
265 for aerosol sizing (Sect. 2.2 and S3), but we do not expect this to affect our overall conclusions as
266 increased aerosol surface area would further reduce n_s (see Results Sect. 3.3 and Discussion Sect.
267 4). Prior to sampling, filters were cleaned by soaking in 10 % peroxide (H_2O_2) for 10 minutes
268 followed by rinsing three times with deionized water, the last rinse further “polished” by passage

269 through a 0.1 μm pore-size syringe filter (Puradisc, Whatman $\text{\textcircled{R}}$, Maidstone, U.K). Filters were
270 pre-loaded into filter units in a laminar flow hood to further minimize contamination from
271 handling. After collection, each aerosol filter was placed in a 60 mm diameter sterile Petri dish
272 (Life Science Products, Frederick, Colorado, USA) using pre-cleaned acetyl plastic forceps (Fine
273 Science Tools, Foster City, California, USA), sealed with Parafilm and stored frozen ($-20\text{ }^{\circ}\text{C}$).
274 Samples were shipped in a dry shipper via Cryoport $\text{\textcircled{R}}$ High Vol Shipper at $-180\text{ }^{\circ}\text{C}$ and upon
275 arrival at the laboratory were stored at $-80\text{ }^{\circ}\text{C}$ until processed, within 18 to 38 months since
276 collection. To release collected particles, filters were immersed in 5-8 mL ultrapure water (Cat.
277 Number W4502, Sigma-Aldrich $\text{\textcircled{R}}$, St. Louis, MO, USA) and shaken by hand for 20 minutes just
278 prior to measurement.

279 INP concentrations were measured using the Scripps Institution of Oceanography Automated Ice
280 Spectrometer (SIO-AIS), an immersion freezing droplet assay instrument that is described in detail
281 in Beall et al. (2017). Briefly, the aerosol sample suspensions and SSW samples were distributed
282 in $30 \times 50\text{-}\mu\text{L}$ aliquots into clean 96-well polypropylene sample trays (OPTIMUM $\text{\textcircled{R}}$ ULTRA
283 Brand, Life Science Products). An equal number and volume of aliquots of ultrapure water
284 accompanied each sample in the tray as a control. Trays were then inserted into an aluminum block
285 that was cooled at $-0.87\text{ }^{\circ}\text{C min}^{-1}$ until the samples froze. Cumulative INP number concentrations
286 per temperature per volume liquid are calculated using the fraction (f) of unfrozen wells per given
287 temperature interval:

$$288$$
$$289 \quad n_{\text{INP,L}} = \frac{-\ln(f)}{V_d} \quad \text{Eq. (1)}$$

290

291 where V_d is the volume of the sample in each well (Vali, 1971). For aerosol filter samples,
292 cumulative INP number concentrations are calculated using the ratio of the ultrapure water volume
293 used for resuspension of the particles (V_{re}) to the volume of air sampled (V_A):

$$294$$
$$295 \quad n_{\text{INP}} = \frac{-\ln(f) \cdot V_{re}}{V_d \cdot V_A} \quad \text{Eq. (2)}$$

296

297 Prior to calculating n_{INP} , the fraction of unfrozen wells (f) was adjusted for contamination in the
 298 water used for suspension by subtracting the number of frozen ultrapure water wells per
 299 temperature interval from both the total number of unfrozen wells and total wells of the sample.
 300 The n_{INP} was additionally adjusted for background INPs from filters and sampling handling
 301 processes. Background n_{INP} were estimated using measured n_{INP} in aerosol sample field blanks,
 302 which had been placed in the sampling apparatus ~ 5 s (without actuating the pump) before removal
 303 and unloading and storage of the filter. Seven field blank samples were collected, one every ~ 7
 304 days of the cruise (Fig. S7). INP concentrations were measured in field blanks as described above,
 305 and the n_{INP} simulated using the mean air volume sampled (6680 L). Figure S7 shows the
 306 estimated n_{INP} across the 7 field blanks, which ranged between 1.0×10^{-4} and $7.0 \times 10^{-3} \text{ L}^{-1}$ at -20
 307 $^{\circ}\text{C}$. The freezing onset temperatures detected in the field blanks ranged between -6 and -27 $^{\circ}\text{C}$. To
 308 correct n_{INP} measured in aerosol samples for background INPs from sample handling, a linear
 309 regression based on the geometric mean n_{INP} measured in field blank suspensions (mL^{-1} water)
 310 was used to estimate background concentrations of INPs in samples at all temperatures between $-$
 311 14.5 $^{\circ}\text{C}$ and -27 $^{\circ}\text{C}$. The estimated background n_{INP} was then subtracted from the INP
 312 concentration measured in filter sample suspension volumes in this temperature range prior to
 313 calculating n_{INP} . The n_{INP} measured in one aerosol sample (f033) fell within the estimated INP
 314 background levels.

315 For this study, the detection limit was $0.68 n_{\text{INP}} \text{ mL}^{-1}$ liquid or 0.001 - $0.0024 n_{\text{INP}} \text{ L}^{-1}$ air for the
 316 minimum and maximum air volume sampled, respectively. To extend the upper limit of detection
 317 (i.e., the point at which all droplets have frozen) dilutions of 1:10 and 1:100 were performed on 8
 318 samples (Fig. S8).

319 The ice-active surface site density, n_s , is a metric used to define the ice-nucleating capabilities of
 320 an aerosol species (i.e., an aerosol sample of all the same particle type) (Kanji et al., 2017) as
 321 follows:

$$322 \quad n_s = \frac{N_{\text{ice}}}{N_{\text{tot}} \times A \text{ (cm}^2\text{)}} \quad \text{Eq. (3)}$$

323 where N_{ice} is the number of frozen droplets, N_{tot} is the total number of particles in a monodisperse
 324 aerosol population, and A is the surface area per particle.

325 The value of n_s can also be approximated for polydisperse aerosol samples containing multiple
326 aerosol types:

$$327 \quad n_s = \frac{N_{ice}}{A_{tot} (cm^2)} \quad \text{Eq. (4)}$$

328 where A_{tot} is the total surface area of the polydisperse aerosol. The difference between the n_s
329 approximation (Eq. 4) and n_s (Eq. 3) is that many particle types are typically included in the n_s
330 approximation, and in an ambient aerosol measurement most of these are not IN-active (see also
331 Hiranuma et al., (2015) Sect. 2.4). Furthermore, the subset of INPs in the sample are likely also of
332 different types, which likely have different n_s in the strict sense (Eq. 3). Nevertheless, the n_s
333 approximation is a useful metric for comparing the ice-nucleating ability of different air masses
334 and source regions and is often used for comparing data across studies of INPs measured in
335 ambient air. It is extremely challenging to separate measurements of INPs and surface area by each
336 particle type, and requires, for example, combining online measurements of single particle
337 chemistry, size distributions and INPs (Cornwell et al., 2019). All n_{INP} and n_s are reported
338 normalized to a standard temperature of 273.15 K and pressure of 1013 hPa.

339 Heat and peroxide treatments were applied to a subset of samples (12 of 26) to test for heat-labile
340 biological (e.g., proteinaceous) and organic INP composition, respectively, following the
341 procedure described in McCluskey et al. (2018b) and Suski et al. (2018). The 12 samples were
342 selected based on sampling location with the aim of getting a representative measurement from
343 each region. For each heat-treated sample, a 2 mL aliquot of the original ultrapure water suspension
344 was heated to 95 °C for 20 min in a water bath and re-tested for changes in n_{INP} . For peroxide
345 treatments, 1.6 mL of the original suspension was combined with 0.8 mL of 30% peroxide (Sigma
346 Aldrich®, St. Louis, Missouri, USA) to achieve a final concentration of 10%, then the mixture
347 was heated to 95 °C for 20 min while being illuminated with two 26-W UVB fluorescent bulbs.
348 To remove residual peroxide and prevent freezing point depression, the solution was cooled and
349 catalase (Cat. Number IC10042910, MP Biomedicals, Santa Ana, California, USA) was added
350 Figure S7 shows the estimated n_{INP} in a heat and peroxide-treated blank sample. Fisher's Exact
351 Test was applied to frozen and unfrozen well fractions between each untreated sample and its
352 corresponding treated sample to test for significant differences ($p < 0.05$). Note that significant
353 difference in frozen well fraction is insufficient as a sole indicator of sensitivity in peroxide treated

354 samples because samples are diluted 2:3 (by 33%) compared to untreated samples. As n_{INP} can be
355 corrected for the dilution by scaling (as opposed to frozen well fractions), the overlap in 95%
356 binomial sampling confidence intervals (Agresti and Coull, 1998) between the untreated and
357 peroxide-treated sample is an additional indicator of sensitivity for a given data point in the
358 peroxide-treated sample spectrum within ± 0.2 °C, the uncertainty in the SIO-AIS temperature
359 measurement (Beall et al., 2021). A lack of overlap in the 95% binomial sampling confidence
360 interval within ± 0.2 °C equates to a significance threshold of $p < 0.005$ (Krzywinski and Altman,
361 2013).

362 INP concentrations were additionally measured in in untreated, heat-treated, and peroxide-treated
363 subsamples from an archived suspension of the soil dust sample N12 SD for comparison with this
364 study (DeMott et al., 2018; hereafter referred to as “N12-SD”). N12 SD (sample CD1 in Megahed
365 2007) is sedimented airborne dust that was carried in boundary layer winds north and then east
366 from the desert in central Egypt during a sandstorm to a sampling point ~50 km north of Cairo,
367 collected on 18th Feb 2003. The sample was stored in a “clean bottle” (no temperature of storage
368 given) for further analysis (Megahed 2007). Briefly, the sample was generated during the recent
369 laboratory intercomparison of INP measurements (collected on a 0.2 μm Nuclepore polycarbonate
370 membrane filter (Whatman®, Chicago, Illinois, USA) and stored frozen at -20 °C until processed,
371 as described in DeMott et al (2018).

372

373 **2.5 INP Measurements in SSW**

374 INP concentrations were additionally measured in 10 SSW samples. For seawater sampling, a
375 water intake vertical steel pipe was positioned on the starboard of the ship approximately 2 m
376 below the sea surface level. The seawater was pumped into a 200 L stainless steel tank and
377 continuously exchanged at a rate of 3000 L h⁻¹. SSW samples for INP analysis were collected in
378 15 mL sterile centrifuge tubes (Falcon™, ThermoFisher Scientific, Waltham, Massachusetts,
379 USA) and stored frozen at -20 °C until they could be shipped in a dry shipper via Cryoport® (-180
380 °C) and ultimately stored at -80 °C as for aerosol samples until processed as described above (Sect.
381 2.4), within 18 to 38 months since collection. Storage duration was not correlated with INP
382 concentration changes in frozen marine and coastal precipitation samples (Beall et al., 2020). Heat
383 and peroxide treatments as described above were applied to 5 SSW samples from the Arabian Sea

384 and the Gulf of Aden. The focus on these regions was motivated by the detection of marine aerosol
385 originating from the upwelling region in Somalia reported in Edtbauer et al., (2020; see Sect.
386 3.3). To assess the contribution of submicron INPs to total measured INPs, 2 mL of SSW was
387 filtered through a 0.2 μm sterile syringe-filter (Acrodisc® Pall®, Port Washington, New York,
388 USA) and re-tested.

389 INP concentrations in SSW collected at the Ellen Browning Scripps Memorial Pier at Scripps
390 Institution of Oceanography (SIO; 32.8662 N, 117.2544 W) were assessed in 17 samples for
391 comparison with SSW collected during AQABA. Samples were collected between 31 Jan and 7
392 May 2016 in 15-30 mL sterile centrifuge tubes (Falcon™, ThermoFisher Scientific, Waltham,
393 Massachusetts, USA) at depths of 1-3m and processed immediately using the SIO-AIS as
394 described above.

395 **3 Results**

396 **3.1 INP Concentrations in Aerosol**

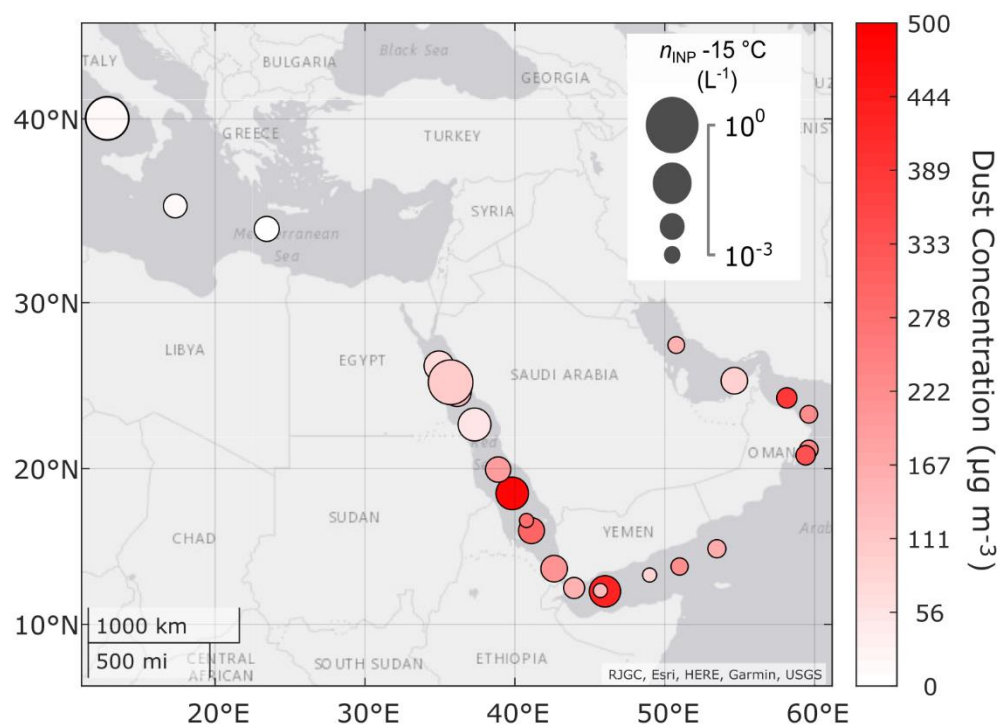
397 A total of 26 aerosol samples were collected in July – August 2017 during AQABA for offline
398 measurements of INPs. The INP concentrations (n_{INP}) measured in samples collected in the
399 Mediterranean Sea, the Red Sea, the Gulf of Aden, Arabian Sea, Gulf of Oman, and Arabian Gulf
400 spanned up to 2 orders of magnitude at $-15\text{ }^{\circ}\text{C}$ (Fig. 1, Table 1), between 5×10^{-3} and $5 \times 10^{-1}\text{ L}^{-1}$.
401 ¹. This range agrees within an order of magnitude with that of Prodi et al. (1983) who measured
402 n_{INP} in the Mediterranean, Red Sea, Gulf of Aden and Indian Ocean nearly 4 decades prior to the
403 present study (4×10^{-2} to 2 L^{-1} at $-16\text{ }^{\circ}\text{C}$). Average ambient dust concentrations during each
404 sampling period ranged from 2-490 $\mu\text{g m}^{-3}$ (PM_{10} Table 1). There is no agreed-upon standard for
405 definition of extreme dust events in the literature, though the 24-hr average WHO or US EPA
406 health standards for average PM_{10} are commonly used (Gandham et al., 2020; Khaniabadi et al.,
407 2017). Using the US EPA health standard for PM_{10} as a threshold for extreme events ($150\text{ }\mu\text{g m}^{-3}$),
408 ³, 14 of the 26 samples were collected during dust events. This is conservative given the equivalent
409 WHO guideline for PM_{10} is $50\text{ }\mu\text{g m}^{-3}$ (WHO, 2005), in which case 22 of the 26 sampling periods

410 would be classified as dust events. Prior studies have reported comparable PM₁₀ levels during dust
411 events in the region (Gandham et al., 2020; Krasnov et al., 2016; Shahsavani et al., 2012).

412 Figs. S9-S10 show the extent of k-means clustered FLEXPART back-trajectories below the
413 altitude of 1500 m (see Sect. S5 for details). This threshold was applied to eliminate most of the
414 free tropospheric parts of the back-trajectories and was selected based on the MERRA-2 monthly
415 average planetary boundary layer (PBL) heights during the campaign period, which were 200-700
416 m over the ocean and up to 1700 m over land. Air mass back trajectories show that source regions
417 included the Mediterranean, Nile Delta, Sinai Peninsula (f006-f008, f038), Northeast Egypt (f009-
418 f010), Iran (f023-f024), and Southern and Eastern Europe (f040, f042, f044) (S9-S16). Many
419 samples collected during extreme dust events (f013, f014, f016, f018, and f020) were influenced
420 by emissions from North Africa and the Arabian Peninsula (Figs S9-S10, S12-14). . The ranges of
421 aerosol surface area concentrations for all sampling periods were < 320 μm² cm⁻³, with the
422 exception of f024, for which aerosol surface area range was > 600 μm² cm⁻³ (Table 1).

423

424



425
 426 **Figure 1.** Map of the sample locations for 26 aerosol samples collected on the RV *Kommandor*
 427 *Iona* during Air Quality and climate change in the Arabian Basin (AQABA; see also Figs. S1-S2
 428 and S9-S10). Measured n_{INP} spanned 2 orders of magnitude at $-15\text{ }^{\circ}\text{C}$, from 5×10^{-3} to 5×10^{-1}
 429 L^{-1} . Marker sizes indicate abundance of INPs. Marker colors indicate the average ambient dust
 430 mass concentration during the sampling period from hourly MERRA-2 reanalysis data.

431
 432 **Table 1.** Summary of aerosol samples collected during AQABA. “—” indicates where data are
 433 missing; “NaN” indicates values below detection limit. Locations are given at the transect
 434 midpoint during each sampling period.

Sample ID	Start datetime (UTC)	Stop datetime (UTC)	Latitude ($^{\circ}$ N)	Longitude ($^{\circ}$ E)	n_{INP} $-15\text{ }^{\circ}\text{C}$ (L^{-1})	Sample Volume (L air)	Average Aerosol Surface Area (PM_{10} , $\mu\text{m}^2 \text{cm}^{-3}$)	Aerosol Surface Area [min, max] (PM_{10} , $\mu\text{m}^2 \text{cm}^{-3}$)	Average Dust Concentration (PM_{10} , $\mu\text{g m}^{-3}$)	Average Seasalt Concentration (PM_{10} , $\mu\text{g m}^{-3}$)
f006	05-Jul 05:46	05-Jul 11:37	26.224	35.025	0.0146	3370	290	[199, 375]	170	-

f007	05-Jul 16:40	05-Jul 19:51	26.291	34.933	0.0475	2588	260	[222, 289]	70	-
f008	06-Jul 07:09	06-Jul 14:08	25.225	35.775	0.1161	5225	177	[106, 259]	100	-
f009	07-Jul 05:50	07-Jul 15:07	25.011	35.947	0.0838	6940	352	[253,416]	110	-
f010	08-Jul 16:33	09-Jul 05:59	23.623	36.931	0.0592	8073	219	[163, 287]	50	-
f013	14-Jul 12:26	14-Jul 16:13	18.687	39.672	0.0585	2283	264	[176, 352]	490	10
f014	15-Jul 05:10	15-Jul 11:49	16.552	40.834	0.0348	4000	271	[204, 343]	300	5
f016	18-Jul 07:04	18-Jul 14:52	11.939	45.334	0.0534	4690	265	[158, 391]	430	-
f018	22-Jul 10:20	22-Jul 18:44	20.941	59.474	0.0166	5025	212	[171, 238]	340	-
f019	23-Jul 04:48	23-Jul 13:34	21.410	59.691	0.0145	5270	218	[190, 240]	240	-
f020	25-Jul 17:15	26-Jul 04:02	23.976	58.809	0.0184	6511	-	-	390	5
f023	04-Aug 04:05	04-Aug 11:56	28.084	50.284	0.0112	4720	835	[756, 965]	150	4
f024	05-Aug 05:57	05-Aug 13:53	25.432	53.853	0.0371	5221	357	[206, 827]	90	-
f025	07-Aug 09:26	07-Aug 16:46	23.814	59.186	0.0129	4410	55	[46, 72]	220	12
f030	13-Aug 07:08	14-Aug 11:06	15.970	54.705	0.0132	15111	28	[16, 144]	160	-
f031	14-Aug 15:03	15-Aug 09:03	14.003	52.357	0.0121	12972	25	[19, 105]	230	-
f032	15-Aug 09:42	15-Aug 15:07	13.354	49.432	0.0059	3260	96	[82, 147]	80	6
f033	16-Aug 09:30	16-Aug 13:17	12.208	45.706	NaN	2280	73	[51, 135]	130	2
f034	16-Aug 13:27	17-Aug 07:04	12.177	45.429	0.0206	8464	168	[51, 372]	150	1
f035	17-Aug 07:30	17-Aug 14:55	13.308	42.974	0.0365	4460	340	[244, 409]	210	2
f036	18-Aug 06:36	18-Aug 15:03	16.290	41.038	0.0057	6634	208	[160, 428]	280	2
f037	19-Aug 07:05	20-Aug 07:04	18.699	39.609	0.0326	18806	240	[175, 331]	190	7
f038	21-Aug 07:22	21-Aug 16:01	24.112	36.554	0.0422	6700	256	[202, 295]	150	-
f040	26-Aug 16:02	27-Aug 07:04	33.803	24.814	0.0314	9030	90	[58, 142]	< 10	3
f042	28-Aug 07:51	28-Aug 16:02	35.310	17.965	0.0279	6396	163	[131, 222]	< 10	2
f044	31-Aug 08:30	31-Aug 20:16	39.569	13.380	0.4572	11296	211	[148, 255]	< 10	-

435 3.2 Seawater Source Potential

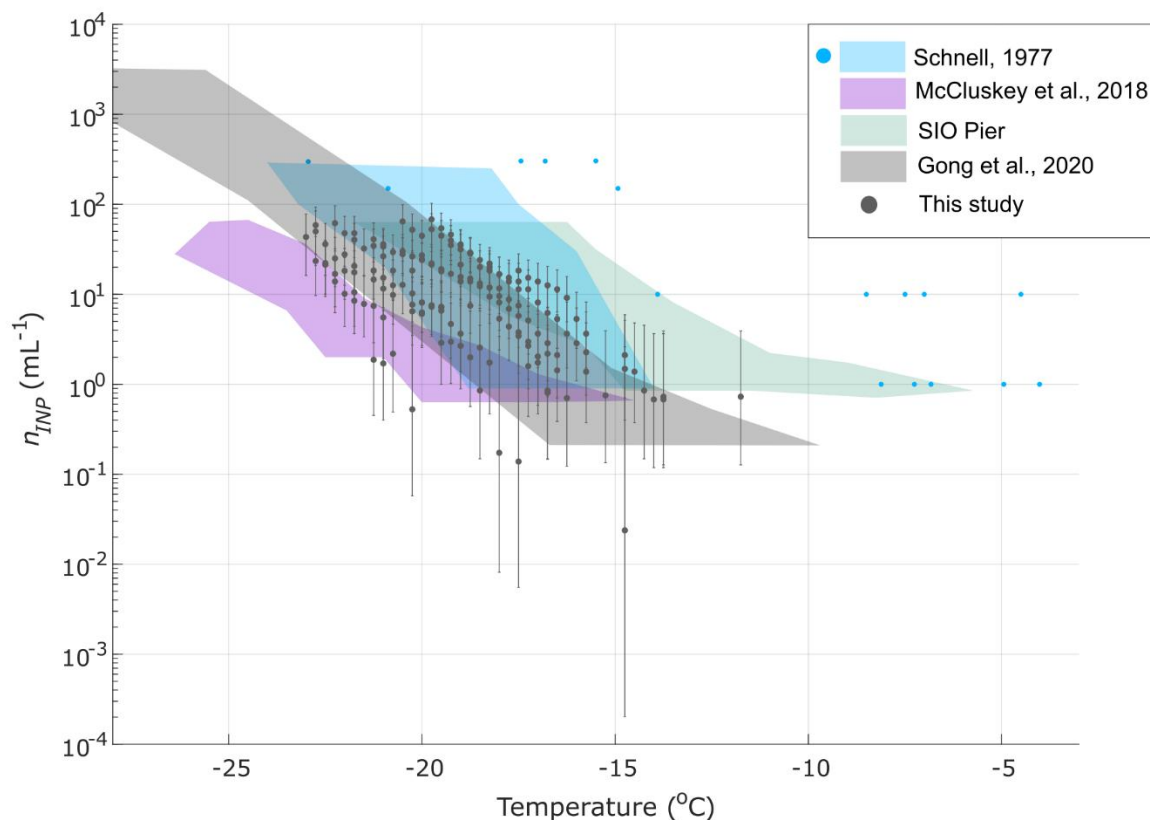
436 The n_{INP} values in 10 SSW samples collected during AQABA were used to characterize the INP
437 source potential of SSA generated by bubble bursting (Wang et al., 2017). Results from prior
438 studies have demonstrated that jet droplets are a more efficient transfer vehicle than film drops of
439 INPs into SSA particles (Mitts et al., 2021; Wang et al., 2017). We measured the n_{INP} in SSW to
440 test whether the seawater source strength was comparable to that of prior studies, or whether the

441 SSW was possibly enriched with INPs due to biological activity or even dust deposition (Cornwell
442 et al., 2020).

443 Figure S17 shows how the n_{INP} measured at $-19\text{ }^{\circ}\text{C}$ in 10 seawater samples varied by the sample
444 collection location. Concentrations ranged between 1 and $50\text{ }n_{\text{INP}}\text{ mL}^{-1}$ and were highest between
445 the Gulf of Oman and the Gulf of Aden. This region exhibited relatively high chlorophyll a during
446 the cruise, with levels between 1 and 30 mg m^{-3} (Fig. S18). In Fig. 2, n_{INP} were compared with
447 SSW from the Ellen Browning Scripps Memorial Pier in coastal Southern California (SIO Pier),
448 Cabo Verde in the Northeast Atlantic, the Southern Ocean (McCluskey et al., 2017), and the
449 Northwest Atlantic (Schnell, 1977). AQABA n_{INP} were most comparable with Gong et al.'s
450 (2020) observations in Cabo Verde. The lack of any unusually high INP spectra suggests that INP
451 enrichment due to dust deposition (Cornwell et al. 2020) was absent or infrequent. It is possible
452 that storage of SSW samples (Sect. 2.5) could have decreased measured n_{INP} , though we expect

453 that n_{INP} would be decreased by no more than $10\times$ in untreated samples stored frozen (see
454 discussion below).

455



456

457 **Figure 2.** Measured n_{INP} in 10 SSW samples collected during AQABA. Also shown are the
458 composite INP spectrum of 14 coastal SSW samples collected on São Vicente Island, Cabo Verde
459 (Gong et al., 2020), 17 coastal SSW samples collected at the Ellen Browning Scripps Pier (green
460 shading), and 12 SSW samples collected in the Southern Ocean (McCluskey et al., 2018d).
461 Schnell's (1977) SSW measurements are represented as a composite spectrum of 24 samples (blue
462 shaded region) and 5 additional spectra (blue markers) from samples that exhibited higher freezing
463 temperatures. All spectra presented are uncorrected for freezing point depression.

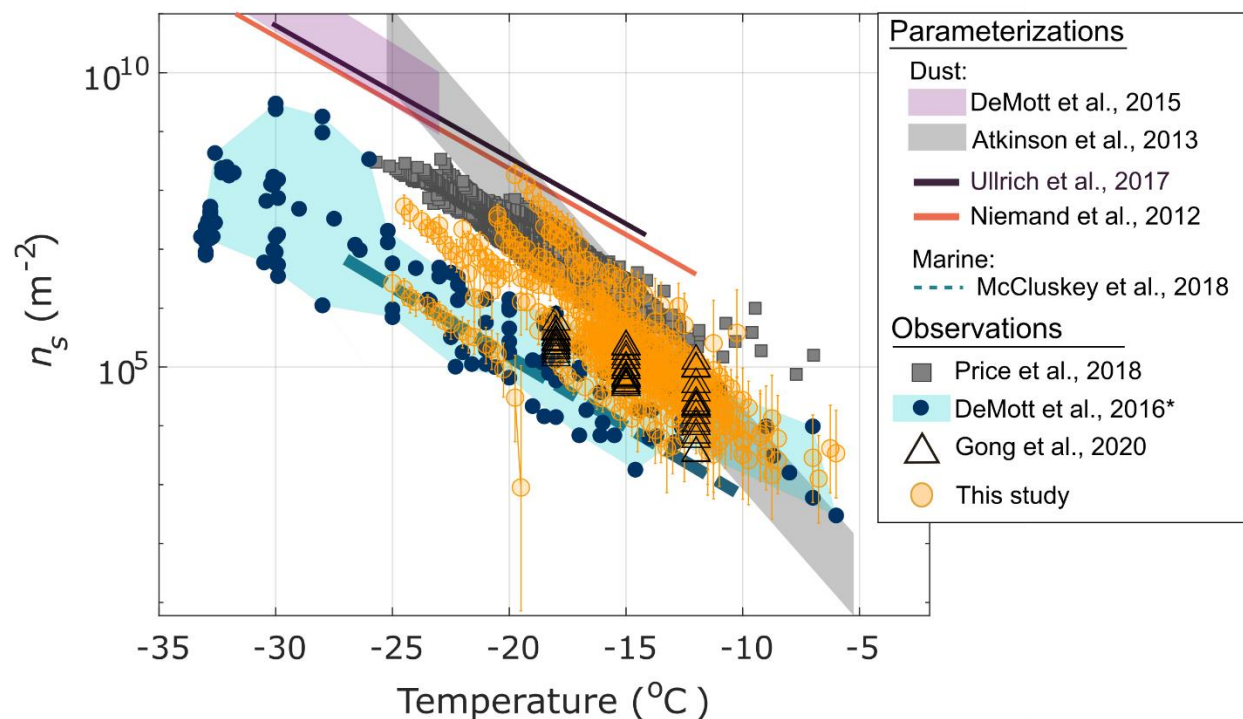
464 Offline treatments for testing heat lability, organic composition, and size were applied to 5 of the
465 10 seawater samples (Methods Sec. 2.5). Heat and $0.2\ \mu\text{m}$ filtering treatments suggest that a large
466 fraction of the seawater INPs were heat sensitive and larger than $0.2\ \mu\text{m}$ (Fig. S19). These results

467 are indicative of the POC type of marine INP defined in McCluskey et al. (2018a), though this
468 result should be interpreted with caution as storage could potentially have increased sensitivity to
469 filtering treatments.

470 Understanding of storage impacts on INPs measured in SSW is lacking. However, Beall et al.,
471 (2020) showed that average INP concentration changes for untreated coastal precipitation samples
472 due to frozen storage were within $2\times$ of n_{INP} measured in fresh samples, with changes at the upper
473 or lower end of the 95% CI exceeding $10\times$ for some freezing temperatures. If SSW samples are
474 similarly sensitive to storage, we would expect INP concentration changes to be within $2\times$ on
475 average, but up to $> 10\times$ for any particular untreated sample. Beall et al. (2020) also reported
476 similar changes INPs $< 0.45 \mu\text{m}$ with a greater tendency toward losses, which indicates that storage
477 may have caused increased sensitivity to the filter treatments applied to stored samples.

478 **3.3 Ice-active Surface Site Densities in Aerosol**

479 In Fig. 3, approximated ice-active surface site densities (n_s) in aerosol samples are compared with
480 multiple population-specific observations and parameterizations for dust and marine INPs. The
481 AQABA measurements are also compared with observations from dust-laden air over the Tropical
482 Atlantic (Price et al., 2018). Overall, observations nearly bridge the full regime between the M18
483 parameterization for marine INPs (McCluskey et al., 2018c), and multiple dust INP
484 parameterizations based on laboratory studies of surface dust. At higher temperatures, between -5
485 and -12 °C, most observations show agreement with the composite spectrum of n_s observed in a
486 range of marine and coastal environments from DeMott et al. (2016) and Yang et al. (2020), and/or
487 the A13 K-feldspar parameterization. Between -10 and -20 °C, several samples agree with the M18
488 marine INP parameterization within an order of magnitude, whereas two to three n_s spectra
489 approach the U17 and N12 laboratory-derived dust INP parameterizations within an order of
490 magnitude (Niemand et al., 2012; Ullrich et al., 2017), depending on temperature. Multiple
491 samples (~8) additionally agreed with Price et al.'s (2018) observations of INPs between 30-3500
492 m above the dust-laden Tropical Atlantic, and most agree with the Gong et al. (2020) surface-level
493 observations, measured at Cabo Verde in the same region as Price et al. (2018).



495

496 **Figure 3.** Ice-active surface site densities (n_s) as a function of temperature for 25 of 26 aerosol
 497 samples collected during AQABA. Gong et al. (2020) and Price et al. (2018) measured INPs in
 498 dust-dominant air masses in the tropical east Atlantic, with minor contributions from SSA, while
 499 the DeMott et al. (2016) measurements were collected across a range of locations and conditions
 500 within the marine boundary layer comprising air masses mostly dominated by relatively pristine
 501 marine SSA. INP concentrations measured in sample f033 were below the detection limits imposed
 502 by field blanks (see Sect. 2.4, Fig. S7). Error bars represent 95% binomial sampling confidence
 503 intervals (Agresti and Coull, 1998). Sample f020 is not shown due to missing aerosol surface area
 504 data during the sampling period. For the 8 samples on which a dilution was performed (Fig. S8),
 505 n_s for both the raw undiluted and diluted sample are shown. *DeMott et al. (2016) data shown have
 506 been updated with additional data from Yang et al. (2020).

507 Considering the frequency of dust events encountered (dust concentration $> 150 \mu\text{g m}^{-3}$, see Table
 508 1), and the high probability that dust was the dominant aerosol source during most sampling
 509 periods, it is striking that most n_s spectra observed are 1-3 orders of magnitude lower than the

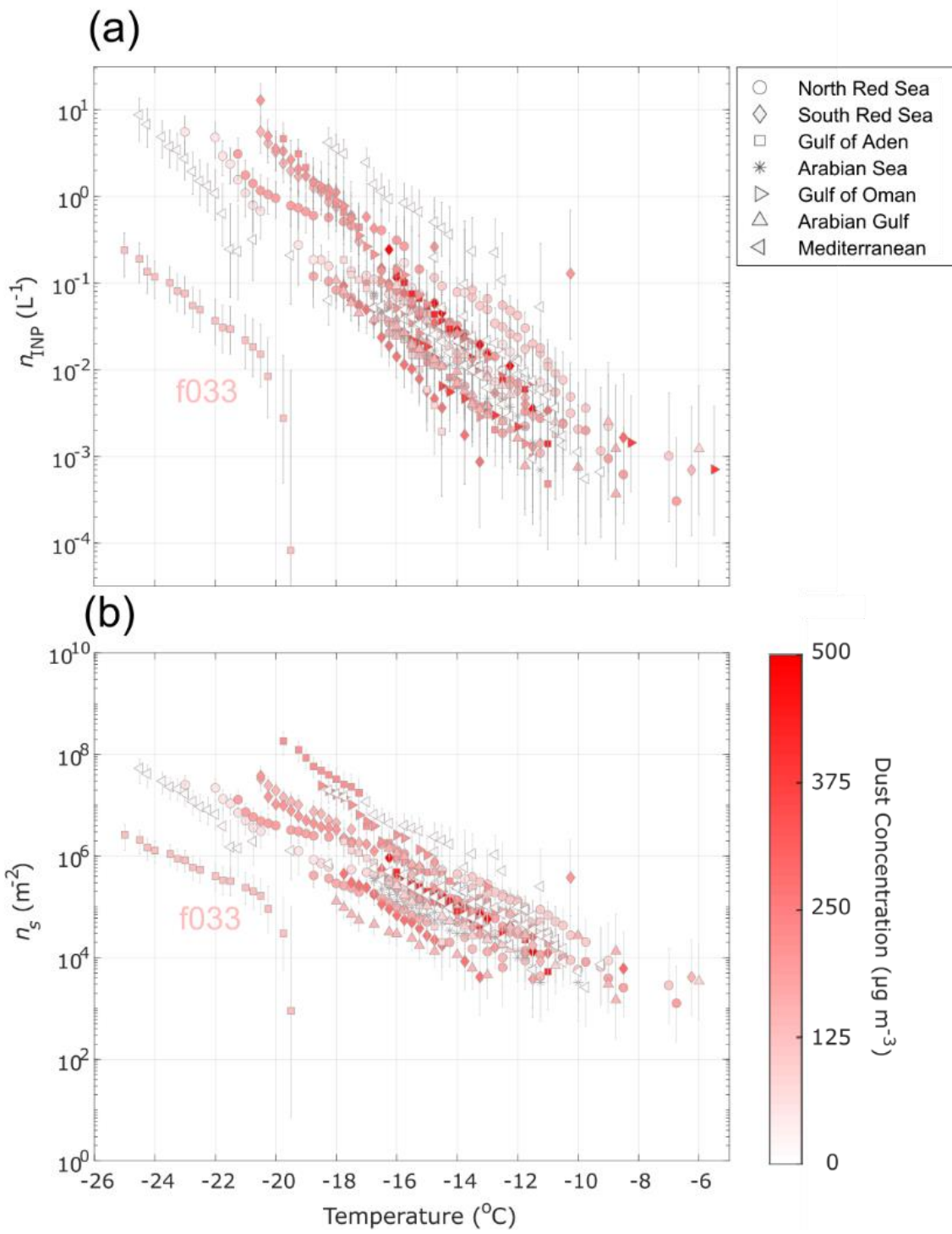
510 values predicted by dust parameterizations. As noted in Gong et al. (2020), some deviations could
511 be expected due to the difference between approximated n_s based on total particle surface area in
512 ambient measurements and true n_s based on surface area of a homogeneous aerosol population (see
513 Methods Sect. 2.4)..

514 Given the marine environment in which sampling took place, a significant amount of sea spray
515 aerosol (SSA) was also detected in many of the sampled airmasses, using sea salt as a proxy (Table
516 1), and likely present in others for which no composition data were available. Edtbauer et al. (2020)
517 reported the detection of high levels of dimethyl sulfide (DMS, up to 800 ppt) in the Gulf of Aden
518 associated with a local phytoplankton bloom during AQABA (as evidenced by visible
519 bioluminescence around the ship at night) as well as high levels of dimethyl sulfone (DMSO₂) and
520 other marine biogenic volatile organic carbons (VOCs) from the Somalian upwelling region. As
521 mentioned above, the n_s for most samples between -6 and -18 °C agree with n_s derived from
522 observations across various locations within the marine boundary layer (Fig. 3). However,
523 considering that SSA is associated with 1000 times fewer IN sites per unit surface area than dust
524 (i.e. 1000× lower n_s) (McCluskey et al., 2018c), the characteristically low IN activity of untreated
525 SSW (even in light of the modest changes expected from storage, Sect. 3.2), and the frequency of
526 dust events during AQABA, our findings suggest it is unlikely that the observed INPs originated
527 from SSA. . In general, detection of marine INPs in ambient aerosol is challenging due to their low
528 relative abundance and decreased efficiency compared to dust (DeMott et al., 2016; McCluskey et
529 al., 2018c). Thus, while SSA contributed to the measured aerosol surface area (Table 1), it is
530 unlikely that the INPs observed in this study were marine in origin, or at least that this is
531 indiscernible in the present study or based on present parameterizations of these populations.

532 Heterogeneous aerosol composition in the sampled air masses likely contributed to some of the
533 low n_s spectra observed due to the contribution of non-INPs to the measured aerosol surface area
534 (see description of n_s approximation in Sect. 2.4). However, the difference between n_s observed
535 during the most extreme dust events, i.e., when the aerosol population was likely approaching
536 homogeneity in composition, and the n_s predicted from N12 and U17 was still greater than 2 orders
537 of magnitude. Figures 4(a) and (b) show overlap in n_{INP} and n_s observed in samples collected in
538 low dust and high dust conditions, indicating that the INP populations observed during AQABA
539 exhibited similar IN activity despite variation in total aerosol composition and dust loading. No

540 correlation was found between n_{INP} and aerosol surface area (Fig. S20), PM_{10} or dust concentration.
541 This result is in contrast to Price et al. (2018) who found the variability in n_{INP} to be largely
542 determined by variability in dust loading or aerosol surface area. Price et al. (2018) reported higher
543 maximum aerosol surface area concentrations of $\sim 1500 \mu\text{m cm}^{-3}$ from three samples collected in
544 an exceptionally optically thick layer, compared to the maximum of $965 \mu\text{m cm}^{-3}$ in the present
545 study (Table 1). Yet overall, the aerosol surface area concentrations compare very well with those
546 observed by (Price et al., 2018), indicative of comparable dustiness in the two studies. Excluding
547 the case mentioned above, the average aerosol surface area was $227 \pm 68 \mu\text{m}^2 \text{cm}^{-3}$ vs. 226 ± 26
548 $\mu\text{m}^2 \text{cm}^{-3}$ for the present study. Furthermore, the sample with the highest n_s at $-15 \text{ }^\circ\text{C}$ (f044) was
549 collected when dust concentrations were lowest ($< 10 \mu\text{g m}^{-3}$) (Fig. 4, Table 1). This is also in

550 direct contrast to Price et al. (2018), who found that the highest n_s observed corresponded to the
551 highest dust loading.



552

553 **Figure 4.** INP concentrations (n_{INP}) **(a)** and ice-active surface site densities (n_s) **(b)** as a function
554 of temperature for 26 aerosol samples collected during AQABA. Markers are colored by the
555 average ambient dust concentration for the respective sampling period. Error bars represent 95%
556 binomial sampling confidence intervals (Agresti and Coull, 1998). The n_s measured in samples
557 collected during low dust conditions are equal to or greater than (up to 100 \times) the n_s measured
558 during dust events between -9 and -18 °C. INP concentrations measured in sample f033 were
559 below the detection limits imposed by field blanks (see Sect. 2.4, Fig. S7). Sample f020 is not
560 shown in (b) due to missing aerosol surface area data during the sampling period. For the 8 samples
561 on which a dilution was performed (Fig. S8), n_s for both the raw undiluted and diluted sample are
562 shown.

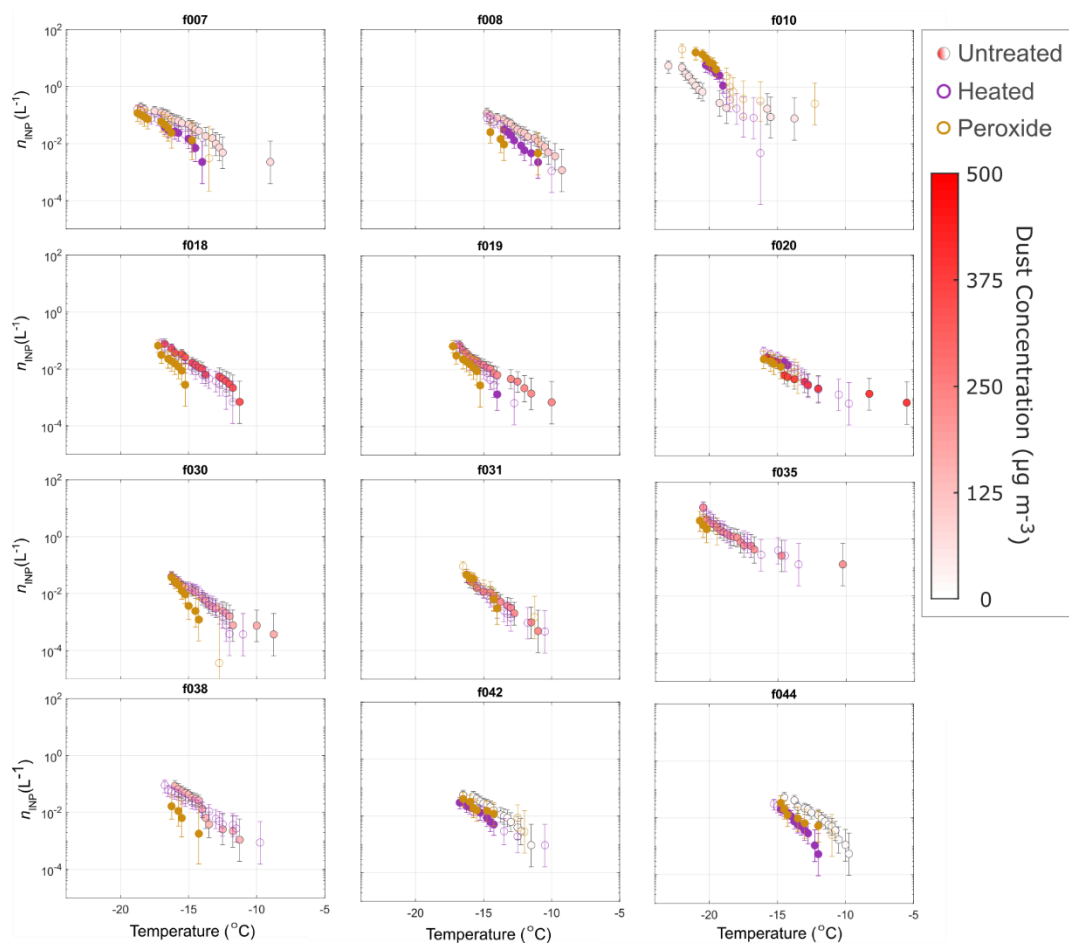
563 **3.4 Characterization of INPs in Aerosol**

564 Offline treatments for testing heat lability and organic composition of INPs were performed on 12
565 samples via heat and peroxide treatments, respectively (Fig. 5). Prior studies have shown that the
566 IN-active component of various types of mineral dusts are insensitive to heat treatments (Conen et
567 al., 2011; Hara et al., 2016; Hill et al., 2016; O’Sullivan et al., 2014). The IN activity of K-feldspar,
568 the dominant ice-nucleating component of mineral dust, was additionally found to be insensitive
569 to digestion with peroxide (O’Sullivan et al., 2014). A small number of studies reported
570 degradation of IN activity with peroxide treatment and/or heat treatment in Arizona Test Dust
571 (ATD), that they attributed to organic material (Perkins et al., 2020; Yadav et al., 2019). Thus, we
572 assume here that any degradation of IN activity due to heat and peroxide treatment correspond to
573 loss of heat-labile (e.g. proteinaceous) and heat-stable organic INPs, respectively.

574 Fisher’s Exact Test was applied to frozen and unfrozen well fractions for each untreated sample
575 and its corresponding treated sample to test for significant differences ($p < 0.05$). Sensitivity to
576 peroxide in most samples (i.e., INP degradation) demonstrate the consistent presence of stable
577 organic INPs at temperatures ≥ -15 °C. The lack of peroxide sensitivity at temperatures < -15 °C
578 indicates dominance by mineral dust INPs at lower temperatures. Heat sensitivity in five samples
579 suggests that biological INPs contributed to their warmest freezing INPs. Gong et al. (2020)
580 similarly found heat-sensitivity in INPs at temperatures > -10 °C. Four of the 12 samples exhibited
581 heat sensitivity at relatively moderate temperatures -11 to -18 °C, including the two samples

582 collected in the Mediterranean Sea. One sample (f010) exhibited increased n_{INP} in freezing
583 temperatures < -18 °C after heat and peroxide treatments. That the response to both heat and
584 peroxide were nearly identical (Fig. 5) suggests that compounds may have been released from the
585 surface during heating, uncovering a more IN active surface underneath (heating was common to
586 both procedures). The increased n_{INP} post heat and peroxide treatment is an unexpected result given
587 previous studies on treated soil dust measurements (Conen et al., 2011; Hill et al., 2016; O’Sullivan
588 et al., 2014; Tobo et al., 2014). However, increases in IN activity after heat treatment have been
589 reported previously for airborne Saharan desert dust and aerosol collected during Saharan dust
590 intrusions (Boose et al., 2019; Conen et al., 2022) as well as SSA and precipitation (Martin et al.,
591 2019; McCluskey et al., 2018a) and should be further investigated in future studies. An increase in

592 IN activity after peroxide treatment has also been reported in a Himalayan dust sample (Paramonov
593 et al., 2018).



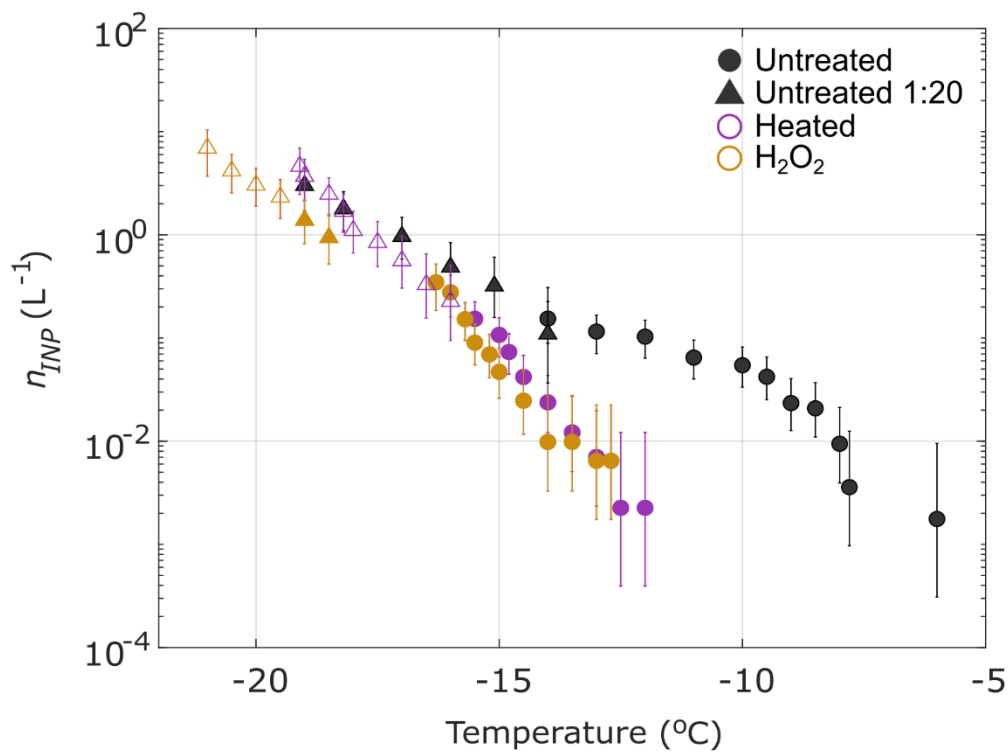
594
595 **Figure 5.** INPs in aerosol samples treated with heat and peroxide (Methods Sec. 2.4) to test for
596 INP heat-lability and organic composition. Markers of untreated spectra are colored by the average
597 dust concentration during the sampling period. Markers of heat-treated and peroxide-treated
598 samples are filled to indicate significant INP concentration difference from untreated samples
599 according to Fisher's Exact Test ($p < 0.05$). Sensitivity to peroxide is evident for all samples $\geq -$
600 15 °C, indicative of stable organic INPs. Heat-lability is also evident at high to moderate
601 temperatures in multiple samples, demonstrating that biological (e.g., proteinaceous) INPs also
602 contributed to INPs observed during AQABA.

603 Given the frequency of dust events and generally high concentrations of dust during most sampling
604 periods, it is surprising that most samples exhibit peroxide sensitivity. Aridisols and entisols are

605 the dominant soil types in North Africa and the Arabian Peninsula (Nortcliff, 2012). Both types
606 are associated with the lowest levels of organic carbon, commonly used as a proxy for total soil
607 organic matter, compared to other soil types (3 and 9 g kg⁻¹, respectively) (Yost and Hartemink,
608 2019).

609 **3.5 Characterization of INPs in a Soil Dust Sample**

610 INP measurements of soil dusts in this region are scarce and have only been reported for a single
611 surface dust soil sample, sample “SD”, collected 50 km north of Cairo (Niemand et al., 2012).
612 FLEXPART back-trajectories indicate this source region for several samples (f006-10, f038),
613 though it should be noted that dust sources cannot be confirmed in this study lacking aerosol and
614 soil dust mineralogy. For comparison with this study, we measured INPs in untreated, heat-treated,
615 and peroxide-treated subsamples of an archived suspension of the N12-SD sample (Methods Sect.
616 2.4; DeMott et al., 2018) . . Sample N12-SD exhibits sensitivity to both heat and peroxide at
617 temperatures > -16 °C, indicating biological composition of INPs at high freezing temperatures.
618 Multiple AQABA samples influenced by desert air mass sources show similar sensitivities at
619 higher temperatures: f006, f007, f019, and f020. Several others exhibit only peroxide-sensitivity
620 in this temperature range. Overall, the heat and peroxide sensitivities in the N12-SD sample
621 indicate that desert dusts may contribute biological and/or organic INPs at moderate to high-
622 freezing temperatures, such as those observed in AQABA samples. Gong et al.'s (2020) results
623 showing heat-sensitivity in INPs at temperatures > -10 °C further demonstrate the contribution of
624 biological INPs at high temperatures in dust-laden air masses near North Africa.



625
 626 **Figure 6.** Measured concentrations of INPs in an aerosolized soil dust sample “N12-SD”, collected
 627 50 km north of Cairo, Egypt (Niemand et al., 2012), that was treated with heat and peroxide to test
 628 for INP heat-lability and organic composition, same as in Fig. 5 above (Methods Sec. 2.4). A 1:20
 629 dilution of the sample is shown (triangles) and markers of heat-treated and peroxide-treated
 630 samples are filled to indicate significant INP concentration differences from untreated samples
 631 according to Fisher’s Exact Test ($p < 0.05$). Sensitivity to peroxide and heat treatments indicates
 632 biological INPs between -6 and -16 °C.

633 4 Discussion

634 Considering the high freezing temperatures observed, evidence of organic composition, and
 635 FLEXPART back trajectories showing that aerosol sources included populous regions and at least
 636 one agriculturally active region (the Nile River Delta; Figs. S9-S16), it is possible that agricultural
 637 soil dusts contributed to some of the relatively higher n_s , n_{INP} , and heat and peroxide sensitivity
 638 observed during AQABA. A range of n_s has been reported in studies of agricultural soil dusts, the
 639 lower end of which agrees with the n_s observed in the present study between -8 and -25 °C (Fig.
 640 3; Steinke et al., 2016; Tobo et al., 2014; O’Sullivan et al., 2014). Samples from air masses

641 influenced by the Nile River Delta or Southern Europe (f007-8, f010, f038, f042, f044) show a
642 higher fraction of heat-sensitive INPs (Fig. 5). Heat-sensitivity is indicative of biological INPs,
643 which have been associated with agricultural soil dusts in prior studies (Hill et al., 2016;
644 O’Sullivan et al., 2014). Hill et al. (2016) and O’Sullivan et al. (2014) showed peroxide sensitivity
645 in agricultural soil dusts at temperatures > -18 to -15 °C, respectively, a range which aligns with
646 the peroxide sensitivity exhibited in the present study.

647 Organic material can condense or adsorb onto aerosols during photochemical and oxidative
648 processes, representing another potential source of organic INPs during AQABA (Dall’Osto et al.,
649 2010; Hinz et al., 2005; Krueger et al., 2004). Could aging explain the organics and decreased n_s
650 observed? Though dust aerosol was collected within 1 day’s transport from source regions
651 throughout this study, we cannot rule out the possibility of aging impacts, lacking single particle
652 chemistry measurements. In addition to field observations of n_{INP} demonstrating that aging
653 increased the IN efficiency of desert dust INPs (see Introduction; Boose et al., 2016; Conen et al.
654 2015), prior studies of the effects of aging on mineral dust INPs have yielded mixed and sometimes
655 contradictory results, indicating that the impact of aging on IN properties likely depends on
656 multiple factors including the ice nucleation pathway, the type of aging process, surface
657 morphology, and mineralogy (Perkins et al., 2020 and references therein). Multiple studies have
658 investigated the effects of various aging processes on Arizona Test Dust (ATD) as a proxy for
659 diverse natural dust samples. These included exposure to sulfuric acid, nitric acid vapor, and
660 solution-phase processes (Cziczo et al., 2009; Eastwood et al., 2009; Knopf and Koop, 2006;
661 Salam et al., 2007; Sullivan et al., 2010b, 2010a). Perkins et al. (2020) demonstrated the INP
662 lability in ATD through multiple solution-phase aging processes (e.g., incubation in water,
663 exposure to acid or salt), with up to 1000× reductions in INP abundance at freezing temperatures
664 > 10 °C. This result contrasts with the increase in IN activity attributed to aging reported in Boose
665 et al. (2016) and Conen et al. (2015). Perkins et al. (2020) additionally reported that the lability of
666 IN activity in ATD is temperature dependent, with large reductions evident at freezing temperature
667 > 10 °C, yet little to no change at temperatures < -15 °C. By contrast, most of the n_s spectra in
668 AQABA samples were 10 – 1000× lower than established dust parameterizations even at
669 temperatures < -15 °C. In summary, it has proven difficult to determine any consistent impact of
670 atmospheric processing on the IN activity of dust in model systems such as ATD (Perkins et al.,
671 2020), and few studies have investigated impacts of aging on ambient desert dust, especially at

672 modest supercooling (Boose et al., 2016). Furthermore, the use of ATD as a proxy for natural dust
673 in INP studies has been questioned due to the complex ice-nucleating properties of natural dust,
674 including mineral composition and defect sites at the particle surface, the latter of which is likely
675 affected by the mechanical processing and milling involved in ATD production (e.g., Perkins et
676 al., 2020 and references therein).

677 Gong et al. (2020) also observed n_s lower by more than 2 orders of magnitude compared to N12
678 and U17 despite the large fraction of supermicron INPs (77-83% depending on temperature), and
679 that the supermicron particles were mainly mineral dust. The cause of the decreased n_s observed
680 here and in Gong et al. (2020) compared to dust n_s parameterizations remains elusive. Both studies
681 were conducted in air masses dominated by dust near major sources. In contrast, Price et al. (2018)
682 found agreement near the region of the Gong et al. (2020) study. One obvious difference is that
683 Price et al. (2018) conducted measurements at higher altitudes, between 30 and 3500 m. A prior
684 study that compared n_{INP} in dust-laden air masses at the surface with n_{INP} collected between 0.5
685 and 3 km above sea level found that median n_{INP} increased by up to $10\times$ above the surface and
686 correlated to dust loading (Schrod et al., 2017). The differences between Price et al. (2018) and
687 the two surface-based studies draws attention to the need for vertical profiles of $n_s > -25$ °C in
688 dust-laden air masses.

689 The decreased n_s compared to Price et al. (2018) is also unlikely to be related to differences in INP
690 measurement. In all three studies, cold stage or droplet assay measurements of immersion mode
691 INPs were used in resuspensions of aerosol collected on filter samples. Recent studies that
692 intercompared instruments designed for measurement of immersion mode INPs showed excellent
693 agreement (i.e., within measurement uncertainty) in measurements of standardized dust and
694 biological samples (DeMott et al., 2018) and when co-sampling ambient aerosol (DeMott et al.,
695 2017). Moreover, the DeMott et al. (2018) intercomparison study demonstrated good agreement
696 in multiple natural dust samples between the various measurement methods used to derive D15,
697 N12 and U17 and the droplet assay methods applied in Gong et al. (2020), Price et al. (2018), and
698 the present study.

699 Storage protocol represents another difference between Price et al. (2018) and the two surface-
700 based studies. Gong et al. (2020) and the present study stored samples frozen prior to analysis,

701 whereas Price et al. (2018) processed samples immediately after collection. An understanding of
702 storage impacts on INPs collected on filters is lacking (Wex et al., 2019), but we note that the
703 discrepancies in n_s between the two surface-based studies and Price et al. (2018) exceed the range
704 of INP concentration changes reported in untreated INP precipitation samples stored frozen (Beall
705 et al., 2020).

706 Thus, the large differences between parameterized n_s for dust, and n_s observed in both Gong et al.
707 (2020) and the present study between -12 and -25 °C indicate that existing n_s -based
708 parameterizations may not faithfully represent n_s at moderate freezing temperatures, despite
709 proximity to major source regions. Whereas DeMott et al. (2015) found that for temperatures < -20
710 °C, mineral dust particles from Saharan and Asian deserts may be parameterized as a common
711 particle type, our findings suggest that characteristic n_s parameterizations for dust from different
712 source regions may be needed > -20 °C, or, alternatively, that this temperature regime requires an
713 alternative to an n_s -based parameterizations. Gong et al. (2019a) demonstrated that predicting n_{INP}
714 from surface area size distributions alone may not be feasible in environments where the aerosol
715 and/or INP composition are unknown and proposed a probability density function (PDF)-based
716 approach to predicting INPs at a given freezing temperature.

717 In light of the evidence from this study that INPs were primarily influenced by organics associated
718 with dust, especially at higher temperatures, and the lack of relationship between dust loading, n_s ,
719 and n_{INP} , we offer the following points for consideration. Prior studies of aerosolized dust
720 demonstrated that it is frequently enriched in organic matter (6-20×) compared to soil dust and that
721 wind erosion selectively removes the chemically-enriched, fine portion of the soil higher in plant
722 nutrients, organic matter and metals (Aryal et al., 2012; Delany and Zenchelsky, 1976; Van Pelt
723 and Zobeck, 2007). Furthermore, a recent study that measured airborne concentrations of
724 prokaryotic cells over the Red Sea characterized the region as a “global hot spot” with average
725 concentrations of 155,000 (\pm 65,000) cells m^{-3} , 19× higher than that over the subtropical and
726 tropical open oceans (Mayol et al., 2014; Yahya et al., 2019). Yahya et al. (2019) demonstrated
727 that the microbial loading was very likely related to the high concentrations of dust, as 99.9% of
728 the cells were attached to dust particles. Organic and biological species have been shown to
729 dominate IN activity at temperatures > ~-15 °C in many studies (e.g., Ladino et al., 2019;
730 O’Sullivan et al., 2018, Kanji et al., 2017, and references therein). Thus, a faithful representation

731 of dust INPs may require two parameterizations: one for the IN activity dominated by minerals <
732 ~ -15 °C such as D15, U17 and N12, and another for the dust-associated organics $> \sim -15$ °C. As
733 IN-active organics are limited compared to the IN-active mineral component of dust, we could
734 expect an increase in n_s slope between warm and cold regimes. The apparent decreased n_s observed
735 in this study between -18 and -12 °C could potentially be related to a plateau in n_s through the
736 transition between the mineral and organic “modes” (see untreated samples in Figs. 5-6). This
737 study underscores the need to characterize the IN-active organic species associated with dust from
738 major source regions and to investigate the extent to which biological and/or organic particles
739 contribute to INP populations in dust-laden air masses at high to moderate freezing temperatures
740 ≥ -15 °C.

741 **5 Conclusions**

742 Observations from the two-month AQABA campaign in the Mediterranean, Red Sea, Arabian Sea
743 and Arabian Gulf are among the first INP measurements made in close proximity to the two largest
744 dust sources globally: the Sahara and the Arabian Peninsula (Kok et al., 2021). Observed n_{INP}
745 measured in 26 aerosol samples spanned 2 orders of magnitude (5×10^{-3} to 5×10^{-1} L $^{-1}$ at -15 °C).

746 In summary, INPs observed during AQABA were very likely dominated by mineral dust with
747 some additional contributions possibly from densely-populated and/or agricultural regions
748 including the Nile River Delta region and Southern or Eastern Europe. Despite proximity to major
749 dust sources and a high frequency of dust events with MERRA-2 simulated mass concentrations
750 up to $490 \mu\text{g m}^{-3}$ (PM $_{10}$), the observed n_s for most samples was lower by 1-3 orders of magnitude
751 compared to n_s predicted by dust parametrizations N12 and U17 at $T < -12$ °C. Observed n_s in 48%
752 of the samples were equivalent within uncertainty to that of the A13 parameterization for K-
753 feldspar (Atkinson et al., 2013), an ice-active component of desert dust. Observed n_s agreed with
754 many observations within the marine boundary layer (DeMott et al., 2016; Yang et al., 2020), and
755 Price et al.'s (2018) measurements of n_{INP} in dust-laden air masses over the Tropical Atlantic,
756 within measurement uncertainty. Peroxide sensitivity was evident in all samples tested (12 of 26),
757 at temperatures ≥ -15 °C, demonstrating a consistent contribution of organic material to warm-
758 temperature INPs. Heat-sensitivity further suggested the presence of biological (e.g.,
759 proteinaceous) INPs in a subset of samples, particularly at high freezing temperatures > -10 °C. A

760 soil dust sample from North Africa (originally from N12) exhibited heat and peroxide sensitivity
761 between -5 and -16 °C, further demonstrating that the IN activity of mineral dust could be
762 associated with organic and/or biological material. Contrary to Price et al. (2018), who measured
763 INP in the dust-laden Tropical Atlantic, no correlation was found between dust loading and n_{INP}
764 or n_s . Results from this study and Gong et al. (2020) indicate that the existing n_s parameterizations
765 alone do not skillfully represent mineral dust associated INPs at modest supercooling near major
766 dust sources.

767 The source strengths of Red Sea, Mediterranean, Arabian Sea, and Arabian Gulf bulk seawater
768 were also evaluated. The maximum source potential was observed in the Arabian Sea (50 INP
769 mL^{-1} at -19 °C.) The observed n_{INP} for SSW samples were equivalent to those of Gong et al.
770 (2020) at Cabo Verde within the 95% binomial sampling confidence intervals (Agresti and Coull,
771 1998).

772 Considering that desert dust parameterizations overpredicted the n_s values observed during
773 AQABA, despite proximity to major global emissions sources, this study demonstrates the need
774 to evaluate the fidelity of dust INP parameterizations in nascent versus aged dust populations.
775 The discrepancies underscore the challenges of evaluating dust-specific INP parameterizations:
776 limited observations at modest supercooling, few assured methods for distinguishing between
777 different INP sources in ambient aerosol, a dearth of characteristic soil dust samples from major
778 dust sources, and limited knowledge of the specific composition and characteristics of dust INPs
779 at temperatures > -15 °C. Vertical profiles of n_s in dust-laden air masses are also needed to
780 determine whether n_s is consistently lower at the surface and examine the variability of n_s with
781 altitude. Potential storage impacts on INPs collected on filters are an additional factor worthy of
782 future investigation, though storage alone does not likely explain the relatively decreased n_s
783 compared to parameterizations observed in this study, as U17 and N12 were both derived from
784 stored dust samples.

785 In addition to providing observations at high to moderate freezing temperatures, future studies
786 could apply the methods developed in Gong et al. (2020) to estimate the contribution of marine
787 INPs to the aerosol sampled by assuming equivalent distributions of sea salt and INPs between
788 seawater and air. Furthermore, given the combination of marine, dust, and anthropogenically-
789 influenced air masses encountered, and the evidence of organic and biological INPs at modest

790 supercooling in this study and Gong et al. (2020), future studies could benefit from advances in
791 on-line Light-Induced Fluorescence (LIF) measurement techniques. Whereas the interpretation of
792 fluorescence data from most LIF-based instruments has been limited by the lack of spectroscopic
793 information, newer instruments support real-time spectrally-resolved size and fluorescence
794 measurement information for single particles (Fennelly et al., 2018; Huffman et al., 2020;
795 Könemann et al., 2019). This information could be used to potentially “tag” different classes of
796 organics and biological aerosols, enabling investigations of relationships between n_s , n_{INP} and
797 organic signatures in, e.g., mineral dusts and agricultural soil dusts. Finally, the decreased n_s
798 observed in this study further motivate comprehensive aerosol-ice nucleation studies, which aim
799 to achieve closure between measured and predicted ambient n_{INP} by simultaneously characterizing
800 ambient INPs and ice nucleation relevant properties of the total aerosol population, such as
801 composition and aerosol chemical mixing state (Sullivan et al., 2007).

802 **Data Availability:** The data set supporting this manuscript is hosted by the UCSD Library
803 Digital Collections (<https://doi.org/10.6075/J0X0676P>) (Beall et al., 2021).

804 **Author contributions:**

805 CMB, TCH, PJD, MOA, CP, JL, JS, FD, BW, HH, MDS, and KAP designed the study. CMB
806 performed the INP measurements, FLEXPART modeling and analysis with support from TCH,
807 PJD, MOA, MDS, MP and KAP. TCH, PJD and MOA contributed significantly to the writing,
808 preparation of figures and analysis. TK, MI, RP and HH supported the field collection of aerosol
809 for INP analysis and TK additionally provided aerosol number concentration data. JS and MP
810 provided aerosol water-soluble composition data. FD oversaw the aerosol sizing and AMS
811 composition measurements and analysis. All authors contributed to the writing of the article.

812 **Competing interests:**

813 The authors declare they have no conflict of interest.

814

815 **Acknowledgements:**

816 The authors acknowledge collaborations with King Abdullah University of Science and
817 Technology (KAUST), the Cyprus Institute (CyI) and the Kuwait Institute for Scientific Research
818 (KISR). We additionally thank Marcel Dorf and Claus Koeppel for the organization of the
819 campaign, as well as Horst Fischer, Ivan Tadic and Uwe Parchatka for provision of the NO data.
820 Analyses and visualizations of dust mass concentrations and Chl *a* used in this paper were
821 produced with the Giovanni online data system, developed and maintained by the NASA GES
822 DISC. Maps throughout this article were created using ArcGIS® software by Esri. We would also
823 like to thank Hays Ships Ltd. and the *Kommandor Iona*'s crew for their attention to the safety and
824 well-being of the researchers. Finally, we thank the three anonymous reviewers whose insightful
825 comments strengthened this paper. Funding was provided by Highly Cited Program at King Saud
826 University and the Max Planck Society and the University of California San Diego (UCSD)
827 Understanding and Protecting the Planet initiative.

828

829

830 **References**

831 Agresti, A. and Coull, B. A.: Approximate Is Better than “Exact” for Interval Estimation of Binomial
832 Proportions, *Am. Stat.*, 52(2), 119, doi:10.2307/2685469, 1998.

833 Ardon-Dryer, K. and Levin, Z.: Ground-based measurements of immersion freezing in the eastern
834 Mediterranean, *Atmos. Chem. Phys.*, 14(10), 5217–5231, doi:10.5194/acp-14-5217-2014, 2014.

835 Aryal, R., Kandel, D., Acharya, D., Chong, M. N. and Beecham, S.: Unusual Sydney dust storm and its
836 mineralogical and organic characteristics, *Environ. Chem.*, 9(6), 537–546 [online] Available from:
837 <https://doi.org/10.1071/EN12131>, 2012.

838 Atkinson, J. D., Murray, B. J., Woodhouse, M. T., Whale, T. F., Baustian, K. J., Carslaw, K. S., Dobbie,
839 S., O’Sullivan, D. and Malkin, T. L.: The importance of feldspar for ice nucleation by mineral dust in
840 mixed-phase clouds, *Nature*, 498(7454), 355–358, doi:10.1038/nature12278, 2013.

841 Beall, C. M., Stokes, M. D., Hill, T. C., DeMott, P. J., DeWald, J. T. and Prather, K. A.: Automation and
842 Heat Transfer Characterization of Immersion Mode Spectroscopy for Analysis of Ice Nucleating
843 Particles, *Atmos. Meas. Tech.*, (February), 1–25, doi:10.5194/amt-2016-412, 2017.

844 Beall, C. M., Lucero, D., Hill, T. C., DeMott, P. J., Stokes, M. D. and Prather, K. A.: Best practices for

845 precipitation sample storage for offline studies of ice nucleation in marine and coastal environments,
846 Atmos. Meas. Tech., 13(12), 6473–6486, doi:10.5194/amt-13-6473-2020, 2020.

847 Beall, C. M., Michaud, J. M., Fish, M. A., Dinasquet, J., Cornwell, G. C., Stokes, M. D., Burkart, M. D.,
848 Hill, T. C., Demott, P. J. and Prather, K. A.: Cultivable halotolerant ice-nucleating bacteria and fungi in
849 coastal precipitation, Atmos. Chem. Phys., 21(11), 9031–9045, doi:10.5194/acp-21-9031-2021, 2021.

850 Boose, Y., Sierau, B., Isabel García, M., Rodríguez, S., Alastuey, A., Linke, C., Schnaiter, M.,
851 Kupiszewski, P., Kanji, Z. A. and Lohmann, U.: Ice nucleating particles in the Saharan Air Layer, Atmos.
852 Chem. Phys., 16(14), 9067–9087, doi:10.5194/acp-16-9067-2016, 2016.

853 Boose, Y., Baloh, P., Plötze, M., Ofner, J., Grothe, H., Sierau, B., Lohmann, U. and Kanji, Z. A.:
854 Heterogeneous ice nucleation on dust particles sourced from nine deserts worldwide -- Part 2: Deposition
855 nucleation and condensation freezing, Atmos. Chem. Phys., 19(2), 1059–1076, doi:10.5194/acp-19-1059-
856 2019, 2019.

857 Bourtsoukidis, E., Ernle, L., Crowley, J. N., Lelieveld, J., Paris, J.-D., Pozzer, A., Walter, D. and
858 Williams, J.: Non-methane hydrocarbon (C_2 – C_8) sources and sinks around the
859 Arabian Peninsula, Atmos. Chem. Phys., 19(10), 7209–7232, doi:10.5194/acp-19-7209-2019, 2019.

860 Bourtsoukidis, E., Pozzer, A., Sattler, T., Matthaios, V. N., Ernle, L., Edtbauer, A., Fischer, H.,
861 Könemann, T., Osipov, S., Paris, J.-D., Pfannerstill, E. Y., Stöner, C., Tadic, I., Walter, D., Wang, N.,
862 Lelieveld, J. and Williams, J.: The Red Sea Deep Water is a potent source of atmospheric ethane and
863 propane, Nat. Commun., 11(1), 447, doi:10.1038/s41467-020-14375-0, 2020.

864 Broadley, S. L., Murray, B. J., Herbert, R. J., Atkinson, J. D., Dobbie, S., Malkin, T. L., Condliffe, E. and
865 Neve, L.: Immersion mode heterogeneous ice nucleation by an illite rich powder representative of
866 atmospheric mineral dust, Atmos. Chem. Phys., 12(1), 287–307, doi:10.5194/acp-12-287-2012, 2012.

867 Brunner, C., Brem, B. T., Collaud Coen, M., Conen, F., Hervo, M., Henne, S., Steinbacher, M., Gysel-
868 Beer, M. and Kanji, Z. A.: The contribution of Saharan dust to the ice-nucleating particle concentrations
869 at the High Altitude Station Jungfrauoch (3580\,m\,a.s.l.), Switzerland, Atmos. Chem. Phys., 21(23),
870 18029–18053, doi:10.5194/acp-21-18029-2021, 2021.

871 Buchard, V., Randles, C. A., da Silva, A. M., Darmenov, A., Colarco, P. R., Govindaraju, R., Ferrare, R.,
872 Hair, J., Beyersdorf, A. J., Ziemba, L. D. and Yu, H.: The MERRA-2 Aerosol Reanalysis, 1980 Onward.
873 Part II: Evaluation and Case Studies, J. Clim., 30(17), 6851–6872, doi:10.1175/JCLI-D-16-0613.1, 2017.

874 Burrows, S. M., Hoose, C., Pöschl, U. and Lawrence, M. G.: Ice nuclei in marine air: biogenic particles or

875 dust?, *Atmos. Chem. Phys.*, 13(1), 245–267, doi:10.5194/acp-13-245-2013, 2013.

876 Celik, S., Drewnick, F., Fachinger, F., Brooks, J., Darbyshire, E., Coe, H., Paris, J.-D., Eger, P. G.,
877 Schuladen, J., Tadic, I., Friedrich, N., Dienhart, D., Hottmann, B., Fischer, H., Crowley, J. N., Harder, H.
878 and Borrmann, S.: Influence of vessel characteristics and atmospheric processes on the gas and particle
879 phase of ship emission plumes: in situ measurements in the Mediterranean Sea and around the Arabian
880 Peninsula, *Atmos. Chem. Phys.*, 20(8), 4713–4734, doi:10.5194/acp-20-4713-2020, 2020.

881 Collins, D. B., Zhao, D. F., Ruppel, M. J., Laskina, O., Grandquist, J. R., Modini, R. L., Stokes, M. D.,
882 Russell, L. M., Bertram, T. H., Grassian, V. H., Deane, G. B. and Prather, K. A.: Direct aerosol chemical
883 composition measurements to evaluate the physicochemical differences between controlled sea spray
884 aerosol generation schemes, *Atmos. Meas. Tech.*, 7(11), 3667–3683, doi:10.5194/amt-7-3667-2014,
885 2014.

886 Conen, F., Morris, C. E., Leifeld, J., Yakutin, M. V and Alewell, C.: Biological residues define the ice
887 nucleation properties of soil dust, *Atmos. Chem. Phys.*, 11(18), 9643–9648, doi:10.5194/acp-11-9643-
888 2011, 2011.

889 Conen, F., Rodríguez, S., Hüglin, C., Henne, S., Herrmann, E., Bukowiecki, N. and Alewell, C.:
890 Atmospheric ice nuclei at the high-altitude observatory Jungfraujoch, Switzerland, *Tellus, Ser. B Chem.*
891 *Phys. Meteorol.*, 67(1), 1–10, doi:10.3402/tellusb.v67.25014, 2015.

892 Conen, F., Einbock, A., Mignani, C. and Hüglin, C.: Measurement report: Ice-nucleating particles active
893 $\geq -15^{\circ}\text{C}$ in free tropospheric air over western Europe, *Atmos. Chem. Phys.*, 22(5), 3433–
894 3444, doi:10.5194/acp-22-3433-2022, 2022.

895 Cornwell, G. C., McCluskey, C. S., Levin, E. J. T., Suski, K. J., DeMott, P. J., Kreidenweis, S. M. and
896 Prather, K. A.: Direct Online Mass Spectrometry Measurements of Ice Nucleating Particles at a California
897 Coastal Site, *J. Geophys. Res. Atmos.*, 124(22), 12157–12172, doi:doi:10.1029/2019JD030466, 2019.

898 Cornwell, G. C., Sultana, C. M., Prank, M., Cochran, R. E., Hill, T. C. J., Schill, G. P., DeMott, P. J.,
899 Mahowald, N. and Prather, K. A.: Ejection of Dust From the Ocean as a Potential Source of Marine Ice
900 Nucleating Particles, *J. Geophys. Res. Atmos.*, 125(24), e2020JD033073,
901 doi:https://doi.org/10.1029/2020JD033073, 2020.

902 Cziczo, D. J., Froyd, K. D., Gallavardin, S. J., Moehler, O., Benz, S., Saathoff, H. and Murphy, D. M.:
903 Deactivation of ice nuclei due to atmospherically relevant surface coatings, *Environ. Res. Lett.*, 4(4),
904 44013, doi:10.1088/1748-9326/4/4/044013, 2009.

905 Dall'Osto, M., Harrison, R. M., Highwood, E. J., O'Dowd, C., Ceburnis, D., Querol, X. and Achterberg,
906 E. P.: Variation of the mixing state of Saharan dust particles with atmospheric transport, *Atmos. Environ.*,
907 44(26), 3135–3146, doi:<https://doi.org/10.1016/j.atmosenv.2010.05.030>, 2010.

908 Delany, A. C. and Zenchelsky, S.: THE ORGANIC COMPONENT OF WIND-EROSION-
909 GENERATED SOIL-DERIVED AEROSOL, *Soil Sci.*, 121(3) [online] Available from:
910 [https://journals.lww.com/soilsci/Fulltext/1976/03000/THE_ORGANIC_COMPONENT_OF_WIND_ER](https://journals.lww.com/soilsci/Fulltext/1976/03000/THE_ORGANIC_COMPONENT_OF_WIND_EROSION_GENERATED.2.aspx)
911 [OSION_GENERATED.2.aspx](https://journals.lww.com/soilsci/Fulltext/1976/03000/THE_ORGANIC_COMPONENT_OF_WIND_EROSION_GENERATED.2.aspx), 1976.

912 Demott, P. J., Prenni, A. J., Mcmeeking, G. R., Sullivan, R. C., Petters, M. D., Tobo, Y., Niemand, M.,
913 Möhler, O., Snider, J. R., Wang, Z. and Kreiden: Integrating laboratory and field data to quantify the
914 immersion freezing ice nucleation activity of mineral dust particles, , 393–409, doi:10.5194/acp-15-393-
915 2015, 2015.

916 DeMott, P. J., Hill, T. C. J., McCluskey, C. S., Prather, K. A., Collins, D. B., Sullivan, R. C., Ruppel, M.
917 J., Mason, R. H., Irish, V. E., Lee, T., Hwang, C. Y., Rhee, T. S., Snider, J. R., McMeeking, G. R.,
918 Dhaniyala, S., Lewis, E. R., Wentzell, J. J. B., Abbatt, J., Lee, C., Sultana, C. M., Ault, A. P., Axson, J.
919 L., Diaz Martinez, M., Venero, I., Santos-Figueroa, G., Stokes, M. D., Deane, G. B., Mayol-Bracero, O.
920 L., Grassian, V. H., Bertram, T. H., Bertram, A. K., Moffett, B. F. and Franc, G. D.: Sea spray aerosol as
921 a unique source of ice nucleating particles, *Proc. Natl. Acad. Sci.*, 113(21), 5797–5803,
922 doi:10.1073/pnas.1514034112, 2016.

923 DeMott, P. J., Hill, T. C. J., Petters, M. D., Bertram, A. K., Tobo, Y., Mason, R. H., Suski, K. J.,
924 McCluskey, C. S., Levin, E. J. T., Schill, G. P., Boose, Y., Rauker, A. M., Miller, A. J., Zaragoza, J.,
925 Rocci, K., Rothfuss, N. E., Taylor, H. P., Hader, J. D., Chou, C., Huffman, J. A., Pöschl, U., Prenni, A. J.
926 and Kreidenweis, S. M.: Comparative measurements of ambient atmospheric concentrations of ice
927 nucleating particles using multiple immersion freezing methods and a continuous flow diffusion chamber,
928 *Atmos. Chem. Phys.*, 17(18), 11227–11245, doi:10.5194/acp-17-11227-2017, 2017.

929 DeMott, P. J., Möhler, O., Cziczo, D. J., Hiranuma, N., Petters, M. D., Petters, S. S., Belosi, F.,
930 Bingemer, H. G., Brooks, S. D., Budke, C., Burkert-Kohn, M., Collier, K. N., Danielczok, A., Eppers, O.,
931 Felgitsch, L., Garimella, S., Grothe, H., Herenz, P., Hill, T. C. J., Höhler, K., Kanji, Z. A., Kiselev, A.,
932 Koop, T., Kristensen, T. B., Krüger, K., Kulkarni, G., Levin, E. J. T., Murray, B. J., Nicosia, A.,
933 O'Sullivan, D., Peckhaus, A., Polen, M. J., Price, H. C., Reicher, N., Rothenberg, D. A., Rudich, Y.,
934 Santachiara, G., Schiebel, T., Schrod, J., Seifried, T. M., Stratmann, F., Sullivan, R. C., Suski, K. J.,
935 Szakáll, M., Taylor, H. P., Ullrich, R., Vergara-Temprado, J., Wagner, R., Whale, T. F., Weber, D., Welti,
936 A., Wilson, T. W., Wolf, M. J. and Zenker, J.: The Fifth International Workshop on Ice Nucleation phase

937 2 (FIN-02): laboratory intercomparison of ice nucleation measurements, *Atmos. Meas. Tech.*, 11(11),
938 6231–6257, doi:10.5194/amt-11-6231-2018, 2018.

939 Eastwood, M. L., Cremel, S., Wheeler, M., Murray, B. J., Girard, E. and Bertram, A. K.: Effects of
940 sulfuric acid and ammonium sulfate coatings on the ice nucleation properties of kaolinite particles,
941 *Geophys. Res. Lett.*, 36(2), doi:<https://doi.org/10.1029/2008GL035997>, 2009.

942 Edtbauer, A., Stöner, C., Pfannerstill, E. Y., Berasategui, M., Walter, D., Crowley, J. N., Lelieveld, J.
943 and Williams, J.: A new marine biogenic emission: methane sulfonamide (MSAM), dimethyl sulfide
944 (DMS), and dimethyl sulfone (DMSO_2) measured in air over the Arabian Sea, *Atmos. Chem.*
945 *Phys.*, 20(10), 6081–6094, doi:10.5194/acp-20-6081-2020, 2020.

946 Eger, P. G., Friedrich, N., Schuladen, J., Shenolikar, J., Fischer, H., Tadic, I., Harder, H., Martinez, M.,
947 Rohloff, R., Tauer, S., Drewnick, F., Fachinger, F., Brooks, J., Darbyshire, E., Sciare, J., Pikridas, M.,
948 Lelieveld, J. and Crowley, J. N.: Shipborne measurements of ClNO_2 in the Mediterranean Sea and
949 around the Arabian Peninsula during summer, *Atmos. Chem. Phys.*, 19(19), 12121–12140,
950 doi:10.5194/acp-19-12121-2019, 2019.

951 Fennelly, M. J., Sewell, G., Prentice, M. B., O’Connor, D. J. and Sodeau, J. R.: Review: The Use of Real-
952 Time Fluorescence Instrumentation to Monitor Ambient Primary Biological Aerosol Particles (PBAP),
953 *Atmosphere (Basel)*, 9(1), doi:10.3390/atmos9010001, 2018.

954 Friedrich, N., Eger, P., Shenolikar, J., Sobanski, N., Schuladen, J., Dienhart, D., Hottmann, B., Tadic, I.,
955 Fischer, H., Martinez, M., Rohloff, R., Tauer, S., Harder, H., Pfannerstill, E. Y., Wang, N., Williams, J.,
956 Brooks, J., Drewnick, F., Su, H., Li, G., Cheng, Y., Lelieveld, J. and Crowley, J. N.: Reactive nitrogen
957 around the Arabian Peninsula and in the Mediterranean Sea during the 2017 AQABA ship campaign,
958 *Atmos. Chem. Phys.*, 21(10), 7473–7498, doi:10.5194/acp-21-7473-2021, 2021.

959 Gandham, H., Dasari, H. P., Langodan, S., Karumuri, R. K. and Hoteit, I.: Major Changes in Extreme
960 Dust Events Dynamics Over the Arabian Peninsula During 2003–2017 Driven by Atmospheric
961 Conditions, *J. Geophys. Res. Atmos.*, 125(24), e2020JD032931,
962 doi:<https://doi.org/10.1029/2020JD032931>, 2020.

963 Gelaro, R., McCarty, W., Suárez, M. J., Todling, R., Molod, A., Takacs, L., Randles, C. A., Darmenov,
964 A., Bosilovich, M. G., Reichle, R., Wargan, K., Coy, L., Cullather, R., Draper, C., Akella, S., Buchard,
965 V., Conaty, A., da Silva, A. M., Gu, W., Kim, G.-K., Koster, R., Lucchesi, R., Merkova, D., Nielsen, J.
966 E., Partyka, G., Pawson, S., Putman, W., Rienecker, M., Schubert, S. D., Sienkiewicz, M. and Zhao, B.:
967 The Modern-Era Retrospective Analysis for Research and Applications, Version 2 (MERRA-2), *J. Clim.*,

968 30(14), 5419–5454, doi:10.1175/JCLI-D-16-0758.1, 2017.

969 Gong, X., Wex, H., Müller, T., Wiedensohler, A., Höhler, K., Kandler, K., Ma, N., Dietel, B., Schiebel,
970 T., Möhler, O. and Stratmann, F.: Characterization of aerosol properties at Cyprus, focusing on cloud
971 condensation nuclei and ice-nucleating particles, *Atmos. Chem. Phys.*, 19(16), 10883–10900,
972 doi:10.5194/acp-19-10883-2019, 2019a.

973 Gong, X., Wex, H., van Pinxteren, M., Triesch, N., Fomba, K. W., Lubitz, J., Stolle, C., Robinson, T.-B.,
974 Müller, T., Herrmann, H. and Stratmann, F.: Ice nucleating particles measured in air, cloud and seawater
975 at the Cape Verde Atmospheric Observatory (CVAO), , doi:10.1594/PANGAEA.906946, 2019b.

976 Gong, X., Wex, H., van Pinxteren, M., Triesch, N., Fomba, K. W., Lubitz, J., Stolle, C., Robinson, T.-B.,
977 Müller, T., Herrmann, H. and Stratmann, F.: Characterization of aerosol particles at Cabo Verde close to
978 sea level and at the cloud level -- Part 2: Ice-nucleating particles in air, cloud and seawater, *Atmos. Chem.*
979 *Phys.*, 20(3), 1451–1468, doi:10.5194/acp-20-1451-2020, 2020.

980 Hara, K., Maki, T., Kakikawa, M., Kobayashi, F. and Matsuki, A.: Effects of different temperature
981 treatments on biological ice nuclei in snow samples, *Atmos. Environ.*, 140, 415–419,
982 doi:10.1016/j.atmosenv.2016.06.011, 2016.

983 Harrison, A. D., Whale, T. F., Carpenter, M. A., Holden, M. A., Neve, L., O’Sullivan, D., Vergara
984 Temprado, J. and Murray, B. J.: Not all feldspars are equal: a survey of ice nucleating properties across
985 the feldspar group of minerals, *Atmos. Chem. Phys.*, 16(17), 10927–10940, doi:10.5194/acp-16-10927-
986 2016, 2016.

987 Harrison, A. D., Lever, K., Sanchez-Marroquin, A., Holden, M. A., Whale, T. F., Tarn, M. D., McQuaid,
988 J. B. and Murray, B. J.: The ice-nucleating ability of quartz immersed in water and its atmospheric
989 importance compared to K-feldspar, *Atmos. Chem. Phys.*, 19(17), 11343–11361, doi:10.5194/acp-19-
990 11343-2019, 2019.

991 Hartmann, M., Adachi, K., Eppers, O., Haas, C., Herber, A., Holzinger, R., Hünerbein, A., Jäkel, E.,
992 Jentsch, C., van Pinxteren, M., Wex, H., Willmes, S. and Stratmann, F.: Wintertime Airborne
993 Measurements of Ice Nucleating Particles in the High Arctic: A Hint to a Marine, Biogenic Source for Ice
994 Nucleating Particles, *Geophys. Res. Lett.*, 47(13), e2020GL087770,
995 doi:https://doi.org/10.1029/2020GL087770, 2020.

996 Hill, T. C. J., DeMott, P. J., Tobo, Y., Fröhlich-Nowoisky, J., Moffett, B. F., Franc, G. D. and
997 Kreidenweis, S. M.: Sources of organic ice nucleating particles in soils, *Atmos. Chem. Phys.*, 16(11),
998 7195–7211, doi:10.5194/acp-16-7195-2016, 2016.

999 Hinz, K.-P., Trimborn, A., Weingartner, E., Henning, S., Baltensperger, U. and Spengler, B.: Aerosol
1000 single particle composition at the Jungfraujoch, *J. Aerosol Sci.*, 36(1), 123–145,
1001 doi:<https://doi.org/10.1016/j.jaerosci.2004.08.001>, 2005.

1002 Hiranuma, N., Augustin-Bauditz, S., Bingemer, H., Budke, C., Curtius, J., Danielczok, A., Diehl, K.,
1003 Dreischmeier, K., Ebert, M., Frank, F., Hoffmann, N., Kandler, K., Kiselev, A., Koop, T., Leisner, T.,
1004 Möhler, O., Nillius, B., Peckhaus, A., Rose, D., Weinbruch, S., Wex, H., Boose, Y., DeMott, P. J., Hader,
1005 J. D., Hill, T. C. J., Kanji, Z. A., Kulkarni, G., Levin, E. J. T., McCluskey, C. S., Murakami, M., Murray,
1006 B. J., Niedermeier, D., Petters, M. D., O’Sullivan, D., Saito, A., Schill, G. P., Tajiri, T., Tolbert, M. A.,
1007 Welti, A., Whale, T. F., Wright, T. P. and Yamashita, K.: A comprehensive laboratory study on the
1008 immersion freezing behavior of illite NX particles: a comparison of 17 ice nucleation measurement
1009 techniques, *Atmos. Chem. Phys.*, 15(5), 2489–2518, doi:10.5194/acp-15-2489-2015, 2015.

1010 Hoose, C. and Möhler, O.: Heterogeneous ice nucleation on atmospheric aerosols: A review of results
1011 from laboratory experiments., 2012.

1012 Hoose, C., Kristjánsson, J. E., Chen, J.-P. and Hazra, A.: A Classical-Theory-Based Parameterization of
1013 Heterogeneous Ice Nucleation by Mineral Dust, Soot, and Biological Particles in a Global Climate Model,
1014 *J. Atmos. Sci.*, 67(8), 2483–2503, doi:10.1175/2010JAS3425.1, 2010.

1015 Huffman, J. A., Perring, A. E., Savage, N. J., Clot, B., Crouzy, B., Tummon, F., Shoshanim, O., Damit,
1016 B., Schneider, J., Sivaprakasam, V., Zawadowicz, M. A., Crawford, I., Gallagher, M., Topping, D.,
1017 Doughty, D. C., Hill, S. C. and Pan, Y.: Real-time sensing of bioaerosols: Review and current
1018 perspectives, *Aerosol Sci. Technol.*, 54(5), 465–495, doi:10.1080/02786826.2019.1664724, 2020.

1019 Huneus, N., Schulz, M., Balkanski, Y., Griesfeller, J., Prospero, J., Kinne, S., Bauer, S., Boucher, O.,
1020 Chin, M., Dentener, F., Diehl, T., Easter, R., Fillmore, D., Ghan, S., Ginoux, P., Grini, A., Horowitz, L.,
1021 Koch, D., Krol, M. C., Landing, W., Liu, X., Mahowald, N., Miller, R., Morcrette, J.-J., Myhre, G.,
1022 Penner, J., Perlwitz, J., Stier, P., Takemura, T. and Zender, C. S.: Global dust model intercomparison in
1023 AeroCom phase I, *Atmos. Chem. Phys.*, 11(15), 7781–7816, doi:10.5194/acp-11-7781-2011, 2011.

1024 Kanji, Z. A., Ladino, L. A., Wex, H., Boose, Y., Burkert-Kohn, M., Cziczo, D. J. and Krämer, M.:
1025 Overview of Ice Nucleating Particles, *Meteorol. Monogr.*, 58, 1.1-1.33, doi:10.1175/amsmonographs-d-
1026 16-0006.1, 2017.

1027 Khaniabadi, Y. O., Daryanoosh, S. M., Amrane, A., Polosa, R., Hopke, P. K., Goudarzi, G., Mohammadi,
1028 M. J., Sicard, P. and Armin, H.: Impact of Middle Eastern Dust storms on human health, *Atmos. Pollut.*
1029 *Res.*, 8(4), 606–613, doi:<https://doi.org/10.1016/j.apr.2016.11.005>, 2017.

1030 Kinne, S., Schulz, M., Textor, C., Guibert, S., Balkanski, Y., Bauer, S. E., Berntsen, T., Berglen, T. F.,
1031 Boucher, O., Chin, M., Collins, W., Dentener, F., Diehl, T., Easter, R., Feichter, J., Fillmore, D., Ghan,
1032 S., Ginoux, P., Gong, S., Grini, A., Hendricks, J., Herzog, M., Horowitz, L., Isaksen, I., Iversen, T.,
1033 Kirkevåg, A., Kloster, S., Koch, D., Kristjansson, J. E., Krol, M., Lauer, A., Lamarque, J. F., Lesins, G.,
1034 Liu, X., Lohmann, U., Montanaro, V., Myhre, G., Penner, J., Pitari, G., Reddy, S., Seland, O., Stier, P.,
1035 Takemura, T. and Tie, X.: An AeroCom initial assessment – optical properties in aerosol component
1036 modules of global models, *Atmos. Chem. Phys.*, 6(7), 1815–1834, doi:10.5194/acp-6-1815-2006, 2006.

1037 Kleist, D. T., Parrish, D. F., Derber, J. C., Treadon, R., Wu, W.-S. and Lord, S.: Introduction of the GSI
1038 into the NCEP Global Data Assimilation System, *Weather Forecast.*, 24(6), 1691–1705,
1039 doi:10.1175/2009WAF2222201.1, 2009.

1040 Klingmüller, K., Pozzer, A., Metzger, S., Stenchikov, G. L. and Lelieveld, J.: Aerosol optical depth trend
1041 over the Middle East, *Atmos. Chem. Phys.*, 16(8), 5063–5073, doi:10.5194/acp-16-5063-2016, 2016.

1042 Knopf, D. A. and Koop, T.: Heterogeneous nucleation of ice on surrogates of mineral dust, *J. Geophys.*
1043 *Res. Atmos.*, 111(D12), doi:https://doi.org/10.1029/2005JD006894, 2006.

1044 Kok, J. F., Adebisi, A. A., Albani, S., Balkanski, Y., Checa-Garcia, R., Chin, M., Colarco, P. R.,
1045 Hamilton, D. S., Huang, Y., Ito, A., Klose, M., Li, L., Mahowald, N. M., Miller, R. L., Obiso, V., Pérez
1046 Garc\'ia-Pando, C., Rocha-Lima, A. and Wan, J. S.: Contribution of the world’s main dust source regions
1047 to the global cycle of desert dust, *Atmos. Chem. Phys.*, 21(10), 8169–8193, doi:10.5194/acp-21-8169-
1048 2021, 2021.

1049 Könemann, T., Savage, N., Klimach, T., Walter, D., Fröhlich-Nowoisky, J., Su, H., Pöschl, U., Huffman,
1050 J. A. and Pöhlker, C.: Spectral Intensity Bioaerosol Sensor (SIBS): an instrument for spectrally resolved
1051 fluorescence detection of single particles in real time, *Atmos. Meas. Tech.*, 12(2), 1337–1363,
1052 doi:10.5194/amt-12-1337-2019, 2019.

1053 Krasnov, H., Katra, I. and Friger, M.: Increase in dust storm related PM10 concentrations: A time series
1054 analysis of 2001–2015, *Environ. Pollut.*, 213, 36–42, doi:https://doi.org/10.1016/j.envpol.2015.10.021,
1055 2016.

1056 Krueger, B. J., Grassian, V. H., Cowin, J. P. and Laskin, A.: Heterogeneous chemistry of individual
1057 mineral dust particles from different dust source regions: the importance of particle mineralogy, *Atmos.*
1058 *Environ.*, 38(36), 6253–6261, doi:https://doi.org/10.1016/j.atmosenv.2004.07.010, 2004.

1059 Krzywinski, M. and Altman, N.: Error bars, *Nat. Methods*, 10(10), 921–922, doi:10.1038/nmeth.2659,
1060 2013.

1061 Ladino, L. A., Raga, G. B., Alvarez-Ospina, H., Andino-Enriquez, M. A., Rosas, I., Martínez, L.,
1062 Salinas, E., Miranda, J., Ramírez-Díaz, Z., Figueroa, B., Chou, C., Bertram, A. K., Quintana, E. T.,
1063 Maldonado, L. A., García-Reynoso, A., Si, M. and Irish, V. E.: Ice-nucleating particles in a coastal
1064 tropical site, *Atmos. Chem. Phys.*, 19(9), 6147–6165, doi:10.5194/acp-19-6147-2019, 2019.

1065 Lohmann, U. and Feichter, J.: Global indirect aerosol effects: a review, *Atmos. Chem. Phys.*, 5(3), 715–
1066 737, doi:10.5194/acp-5-715-2005, 2005.

1067 Manders, A. M. ., Schapp, M., Jozwicka, M., van Arkel, F., Weijers, E. . and Matthijsen, J.: The
1068 contribution of sea salt to PM 10 and PM in the Netherlands, [online] Available from:
1069 <http://www.pbl.nl/sites/default/files/cms/publicaties/500099004.pdf>, 2009.

1070 Martin, A. C., Cornwell, G., Beall, C. M., Cannon, F., Reilly, S., Schaap, B., Lucero, D., Creamean, J.,
1071 Ralph, F. M., Mix, H. T. and Prather, K.: Contrasting local and long-range-transported warm ice-
1072 nucleating particles during an atmospheric river in coastal California, USA, *Atmos. Chem. Phys.*, 19(7),
1073 4193–4210, doi:10.5194/acp-19-4193-2019, 2019.

1074 Mayol, E., Jiménez, M. A., Herndl, G. J., Duarte, C. M. and Arrieta, J. M.: Resolving the abundance and
1075 air-sea fluxes of airborne microorganisms in the North Atlantic Ocean, *Front. Microbiol.*, 5, 557,
1076 doi:10.3389/fmicb.2014.00557, 2014.

1077 McCluskey, C. S., Hill, T. C. J., Malfatti, F., Sultana, C. M., Lee, C., Santander, M. V, Beall, C. M.,
1078 Moore, K. A., Cornwell, G. C., Collins, D. B., Prather, K. A., Jayarathne, T., Stone, E. A., Azam, F.,
1079 Kreidenweis, S. M. and DeMott, P. J.: A Dynamic Link between Ice Nucleating Particles Released in
1080 Nascent Sea Spray Aerosol and Oceanic Biological Activity during Two Mesocosm Experiments, *J.*
1081 *Atmos. Sci.*, 74(1), 151–166, doi:10.1175/JAS-D-16-0087.1, 2017.

1082 McCluskey, C. S., Hill, T. C. J., Sultana, C. M., Laskina, O., Trueblood, J., Santander, M. V., Beall, C.
1083 M., Michaud, J. M., Kreidenweis, S. M., Prather, K. A., Grassian, V., DeMott, P. J., McCluskey, C. S.,
1084 Hill, T. C. J., Sultana, C. M., Laskina, O., Trueblood, J., Santander, M. V., Beall, C. M., Michaud, J. M.,
1085 Kreidenweis, S. M., Prather, K. A., Grassian, V. and DeMott, P. J.: A mesocosm double feature: Insights
1086 into the chemical make-up of marine ice nucleating particles, *J. Atmos. Sci.*, JAS-D-17-0155.1,
1087 doi:10.1175/JAS-D-17-0155.1, 2018a.

1088 McCluskey, C. S., Hill, T. C. J., Sultana, C. M., Laskina, O., Trueblood, J., Santander, M. V, Beall, C.
1089 M., Michaud, J. M., Kreidenweis, S. M., Prather, K. A., Grassian, V. and DeMott, P. J.: A Mesocosm
1090 Double Feature: Insights into the Chemical Makeup of Marine Ice Nucleating Particles, *J. Atmos. Sci.*,
1091 75(7), 2405–2423, doi:10.1175/JAS-D-17-0155.1, 2018b.

1092 McCluskey, C. S., Ovadnevaite, J., Rinaldi, M., Atkinson, J., Belosi, F., Ceburnis, D., Marullo, S., Hill,
1093 T. C. J., Lohmann, U., Kanji, Z. A., O'Dowd, C., Kreidenweis, S. M. and DeMott, P. J.: Marine and
1094 Terrestrial Organic Ice-Nucleating Particles in Pristine Marine to Continentally Influenced Northeast
1095 Atlantic Air Masses, *J. Geophys. Res. Atmos.*, 123(11), 6196–6212, doi:10.1029/2017JD028033, 2018c.

1096 McCluskey, C. S., Hill, T. C. J., Humphries, R. S., Rauker, A. M., Moreau, S., Stratton, P. G., Chambers,
1097 S. D., Williams, A. G. and McRobert, I.: Observations of Ice Nucleating Particles Over Southern Ocean
1098 Waters, *Geophys. Res. Lett.*, 989–997, doi:10.1029/2018GL079981, 2018d.

1099 Megahed, K., 2007: The impact of mineral dust aerosol particles on cloud formation. Ph.D. dissertation,
1100 Rheinische Friedrich-Wilhelms-University Bonn, 175 pp. [Available online at [https://bonndoc.ulb.uni-](https://bonndoc.ulb.uni-bonn.de/xmlui/handle/20.500.11811/3083)
1101 [bonn.de/xmlui/handle/20.500.11811/3083](https://bonndoc.ulb.uni-bonn.de/xmlui/handle/20.500.11811/3083)]

1102 Mitts, B., Wang, X., Lucero, D., Beall, C., Deane, G., DeMott, P. and Prather, K.: Importance of
1103 Supermicron Ice Nucleating Particles in Nascent Sea Spray, *Geophys. Res. Lett.*, n/a(n/a),
1104 e2020GL089633, doi:https://doi.org/10.1029/2020GL089633, 2021.

1105 Molod, A., Takacs, L., Suarez, M. and Bacmeister, J.: Development of the GEOS-5 atmospheric general
1106 circulation model: evolution from MERRA to MERRA2, *Geosci. Model Dev.*, 8(5), 1339–1356,
1107 doi:10.5194/gmd-8-1339-2015, 2015.

1108 Murray, B. J., O'Sullivan, D., Atkinson, J. D. and Webb, M. E.: Ice nucleation by particles immersed in
1109 supercooled cloud droplets., *Chem. Soc. Rev.*, 41(19), 6519–54, doi:10.1039/c2cs35200a, 2012.

1110 Nickovic, S., Vukovic, A., Vujadinovic, M., Djurdjevic, V. and Pejanovic, G.: Technical Note: High-
1111 resolution mineralogical database of dust-productive soils for atmospheric dust modeling, *Atmos. Chem.*
1112 *Phys.*, 12(2), 845–855, doi:10.5194/acp-12-845-2012, 2012.

1113 Niedermeier, D., Augustin-Bauditz, S., Hartmann, S., Wex, H., Ignatius, K. and Stratmann, F.: Can we
1114 define an asymptotic value for the ice active surface site density for heterogeneous ice nucleation?, *J.*
1115 *Geophys. Res. Atmos.*, 120(10), 5036–5046, doi:https://doi.org/10.1002/2014JD022814, 2015.

1116 Niemand, M., Möhler, O., Vogel, B., Vogel, H., Hoose, C., Connolly, P., Klein, H., Bingemer, H.,
1117 Demott, P., Skrotzki, J. and Leisner, T.: A particle-surface-area-based parameterization of immersion
1118 freezing on desert dust particles, *J. Atmos. Sci.*, 69(10), 3077–3092, doi:10.1175/JAS-D-11-0249.1, 2012.

1119 Nortcliff, S.: *World Soil Resources and Food Security*. Edited by R. Lal and BA Stewart. Boca Raton, FL,
1120 USA: CRC Press (2012), pp. 574, £82.00. ISBN-13: 978-1439844502., *Exp. Agric.*, 48(2), 305–306,
1121 2012.

1122 O’Sullivan, D., Murray, B. J., Malkin, T. L., Whale, T. F., Umo, N. S., Atkinson, J. D., Price, H. C.,
1123 Baustian, K. J., Browse, J. and Webb, M. E.: Ice nucleation by fertile soil dusts: relative importance of
1124 mineral and biogenic components, *Atmos. Chem. Phys.*, 14(4), 1853–1867, doi:10.5194/acp-14-1853-
1125 2014, 2014.

1126 O’Sullivan, D., Adams, M. P., Tarn, M. D., Harrison, A. D., Vergara-Temprado, J., Porter, G. C. E.,
1127 Holden, M. A., Sanchez-Marroquin, A., Carotenuto, F., Whale, T. F., McQuaid, J. B., Walshaw, R.,
1128 Hedges, D. H. P., Burke, I. T., Cui, Z. and Murray, B. J.: Contributions of biogenic material to the
1129 atmospheric ice-nucleating particle population in North Western Europe, *Sci. Rep.*, 8(1), 13821,
1130 doi:10.1038/s41598-018-31981-7, 2018.

1131 Paramonov, M., David, R. O., Kretzschmar, R. and Kanji, Z. A.: A laboratory investigation of the ice
1132 nucleation efficiency of three types of mineral and soil dust, *Atmos. Chem. Phys.*, 18(22), 16515–16536,
1133 doi:10.5194/acp-18-16515-2018, 2018.

1134 Van Pelt, R. S. and Zobeck, T. M.: Chemical Constituents of Fugitive Dust, *Environ. Monit. Assess.*,
1135 130(1), 3–16, doi:10.1007/s10661-006-9446-8, 2007.

1136 Perkins, R. J., Gillette, S. M., Hill, T. C. J. and DeMott, P. J.: The Labile Nature of Ice Nucleation by
1137 Arizona Test Dust, *ACS Earth Sp. Chem.*, 4(1), 133–141, doi:10.1021/acsearthspacechem.9b00304,
1138 2020.

1139 Pfannerstill, E. Y., Wang, N., Edtbauer, A., Bourtsoukidis, E., Crowley, J. N., Dienhart, D., Eger, P. G.,
1140 Ernle, L., Fischer, H., Hottmann, B., Paris, J.-D., Stöner, C., Tadic, I., Walter, D., Lelieveld, J. and
1141 Williams, J.: Shipborne measurements of total OH reactivity around the Arabian Peninsula and its role in
1142 ozone chemistry, *Atmos. Chem. Phys.*, 19(17), 11501–11523, doi:10.5194/acp-19-11501-2019, 2019.

1143 Price, H. C., Baustian, K. J., McQuaid, J. B., Blyth, A., Bower, K. N., Choularton, T., Cotton, R. J., Cui,
1144 Z., Field, P. R., Gallagher, M., Hawker, R., Merrington, A., Miltenberger, A., Neely III, R. R., Parker, S.
1145 T., Rosenberg, P. D., Taylor, J. W., Trembath, J., Vergara-Temprado, J., Whale, T. F., Wilson, T. W.,
1146 Young, G. and Murray, B. J.: Atmospheric Ice-Nucleating Particles in the Dusty Tropical Atlantic, *J.*
1147 *Geophys. Res. Atmos.*, 123(4), 2175–2193, doi:https://doi.org/10.1002/2017JD027560, 2018.

1148 Prodi, F., Santachiara, G. and Oliosì, F.: Characterization of aerosols in marine environments
1149 (Mediterranean, Red Sea, and Indian Ocean), *J. Geophys. Res. Ocean.*, 88(C15), 10957–10968,
1150 doi:https://doi.org/10.1029/JC088iC15p10957, 1983.

1151 Rienecker, M. M., Suarez, M. J., Gelaro, R., Todling, R., Bacmeister, J., Liu, E., Bosilovich, M. G.,
1152 Schubert, S. D., Takacs, L., Kim, G.-K., Bloom, S., Chen, J., Collins, D., Conaty, A., da Silva, A., Gu,

1153 W., Joiner, J., Koster, R. D., Lucchesi, R., Molod, A., Owens, T., Pawson, S., Pegion, P., Redder, C. R.,
1154 Reichle, R., Robertson, F. R., Ruddick, A. G., Sienkiewicz, M. and Woollen, J.: MERRA: NASA's
1155 Modern-Era Retrospective Analysis for Research and Applications, *J. Clim.*, 24(14), 3624–3648,
1156 doi:10.1175/JCLI-D-11-00015.1, 2011.

1157 Salam, A., Lohmann, U. and Lesins, G.: Ice nucleation of ammonia gas exposed montmorillonite mineral
1158 dust particles, *Atmos. Chem. Phys.*, 7(14), 3923–3931, doi:10.5194/acp-7-3923-2007, 2007.

1159 Schnell, R. C.: Ice Nuclei in Seawater, Fog Water and Marine Air off the Coast of Nova Scotia: Summer
1160 1975, *J. Atmos. Sci.*, 34(8), 1299–1305, doi:10.1175/1520-0469(1977)034<1299:INISFW>2.0.CO;2,
1161 1977.

1162 Schrod, J., Weber, D., Drücke, J., Keleshis, C., Pikridas, M., Ebert, M., Cvetković, B., Nickovic, S.,
1163 Marinou, E., Baars, H., Ansmann, A., Vrekoussis, M., Mihalopoulos, N., Sciare, J., Curtius, J. and
1164 Bingemer, H. G.: Ice nucleating particles over the Eastern Mediterranean measured by unmanned aircraft
1165 systems, *Atmos. Chem. Phys.*, 17(7), 4817–4835, doi:10.5194/acp-17-4817-2017, 2017.

1166 Shahsavani, A., Naddafi, K., Jafarzade Haghighifard, N., Mesdaghinia, A., Yunesian, M., Nabizadeh, R.,
1167 Arahami, M., Sowlat, M. H., Yarahmadi, M., Saki, H., Alimohamadi, M., Nazmara, S., Motevalian, S. A.
1168 and Goudarzi, G.: The evaluation of PM₁₀, PM_{2.5}, and PM₁ concentrations during the Middle Eastern
1169 Dust (MED) events in Ahvaz, Iran, from april through september 2010, *J. Arid Environ.*, 77, 72–83,
1170 doi:https://doi.org/10.1016/j.jaridenv.2011.09.007, 2012.

1171 Sullivan, R. C., Guazzotti, S. A., Sodeman, D. A. and Prather, K. A.: Direct observations of the
1172 atmospheric processing of Asian mineral dust, *Atmos. Chem. Phys.*, 7(5), 1213–1236, doi:10.5194/acp-7-
1173 1213-2007, 2007.

1174 Sullivan, R. C., Miñambres, L., DeMott, P. J., Prenni, A. J., Carrico, C. M., Levin, E. J. T. and
1175 Kreidenweis, S. M.: Chemical processing does not always impair heterogeneous ice nucleation of mineral
1176 dust particles, *Geophys. Res. Lett.*, 37(24), doi:https://doi.org/10.1029/2010GL045540, 2010a.

1177 Sullivan, R. C., Petters, M. D., DeMott, P. J., Kreidenweis, S. M., Wex, H., Niedermeier, D., Hartmann,
1178 S., Clauss, T., Stratmann, F., Reitz, P., Schneider, J. and Sierau, B.: Irreversible loss of ice nucleation
1179 active sites in mineral dust particles caused by sulphuric acid condensation, *Atmos. Chem. Phys.*, 10(23),
1180 11471–11487, doi:10.5194/acp-10-11471-2010, 2010b.

1181 Suski, K. J., Hill, T. C. J., Levin, E. J. T., Miller, A., DeMott, P. J. and Kreidenweis, S. M.: Agricultural
1182 harvesting emissions of ice-nucleating particles, *Atmos. Chem. Phys.*, 18(18), 13755–13771,
1183 doi:10.5194/acp-18-13755-2018, 2018.

1184 Tadic, I., Crowley, J. N., Dienhart, D., Eger, P., Harder, H., Hottmann, B., Martinez, M., Parchatka, U.,
1185 Paris, J.-D., Pozzer, A., Rohloff, R., Schuladen, J., Shenolikar, J., Tauer, S., Lelieveld, J. and Fischer, H.:
1186 Net ozone production and its relationship to nitrogen oxides and volatile organic compounds in the
1187 marine boundary layer around the Arabian Peninsula, *Atmos. Chem. Phys.*, 20(11), 6769–6787,
1188 doi:10.5194/acp-20-6769-2020, 2020.

1189 Tobo, Y., DeMott, P. J., Hill, T. C. J., Prenni, A. J., Swoboda-Colberg, N. G., Franc, G. D. and
1190 Kreidenweis, S. M.: Organic matter matters for ice nuclei of agricultural soil origin, *Atmos. Chem. Phys.*,
1191 14(16), 8521–8531, doi:10.5194/acp-14-8521-2014, 2014.

1192 Ullrich, R., Hoose, C., Möhler, O., Niemand, M., Wagner, R., Höhler, K., Hiranuma, N., Saathoff, H. and
1193 Leisner, T.: A new ice nucleation active site parameterization for desert dust and soot, *J. Atmos. Sci.*,
1194 74(3), 699–717, doi:10.1175/JAS-D-16-0074.1, 2017.

1195 Vali, G.: Quantitative Evaluation of Experimental Results an the Heterogeneous Freezing Nucleation of
1196 Supercooled Liquids, *J. Atmos. Sci.*, 28(3), 402–409, doi:10.1175/1520-
1197 0469(1971)028<0402:QEOERA>2.0.CO;2, 1971.

1198 Vergara-Temprado, J., Murray, B. J., Wilson, T. W., O’Sullivan, D., Browse, J., Pringle, K. J., Ardon-
1199 Dryer, K., Bertram, A. K., Burrows, S. M., Ceburnis, D., Demott, P. J., Mason, R. H., O’Dowd, C. D.,
1200 Rinaldi, M. and Carslaw, K. S.: Contribution of feldspar and marine organic aerosols to global ice
1201 nucleating particle concentrations, *Atmos. Chem. Phys.*, 17(5), 3637–3658, doi:10.5194/acp-17-3637-
1202 2017, 2017.

1203 Vergara-Temprado, J., Miltenberger, A. K., Furtado, K., Grosvenor, D. P., Shipway, B. J., Hill, A. A.,
1204 Wilkinson, J. M., Field, P. R., Murray, B. J. and Carslaw, K. S.: Strong control of Southern Ocean cloud
1205 reflectivity by ice-nucleating particles, *Proc. Natl. Acad. Sci.*, 115(11), 2687 LP – 2692,
1206 doi:10.1073/pnas.1721627115, 2018.

1207 Wang, N., Edtbauer, A., Stöner, C., Pozzer, A., Bourtsoukidis, E., Ernle, L., Dienhart, D., Hottmann, B.,
1208 Fischer, H., Schuladen, J., Crowley, J. N., Paris, J.-D., Lelieveld, J. and Williams, J.: Measurements of
1209 carbonyl compounds around the Arabian Peninsula: overview and model comparison, *Atmos. Chem.*
1210 *Phys.*, 20(18), 10807–10829, doi:10.5194/acp-20-10807-2020, 2020.

1211 Wang, X., Deane, G. B., Moore, K. A., Ryder, O. S., Stokes, M. D., Beall, C. M., Collins, D. B.,
1212 Santander, M. V., Burrows, S. M., Sultana, C. M. and Prather, K. A.: The role of jet and film drops in
1213 controlling the mixing state of submicron sea spray aerosol particles, *Proc. Natl. Acad. Sci.*, 114(27),
1214 6978–6983, doi:10.1073/pnas.1702420114, 2017.

1215 von der Weiden, S.-L., Drewnick, F. and Borrmann, S.: Particle Loss Calculator – a new software tool for
1216 the assessment of the performance of aerosol inlet systems, *Atmos. Meas. Tech.*, 2(2), 479–494,
1217 doi:10.5194/amt-2-479-2009, 2009.

1218 Welti, A., Lüönd, F., Kanji, Z. A., Stetzer, O. and Lohmann, U.: Time dependence of immersion freezing:
1219 an experimental study on size selected kaolinite particles, *Atmos. Chem. Phys.*, 12(20), 9893–9907,
1220 doi:10.5194/acp-12-9893-2012, 2012.

1221 Wex, H., DeMott, P. J., Tobo, Y., Hartmann, S., Rösch, M., Clauss, T., Tomsche, L., Niedermeier, D. and
1222 Stratmann, F.: Kaolinite particles as ice nuclei: learning from the use of different kaolinite samples and
1223 different coatings, *Atmos. Chem. Phys.*, 14(11), 5529–5546, doi:10.5194/acp-14-5529-2014, 2014.

1224 Wex, H., Huang, L., Zhang, W., Hung, H., Traversi, R., Becagli, S., Sheesley, R. J., Moffett, C. E.,
1225 Barrett, T. E., Bossi, R., Skov, H., Hünerbein, A., Lubitz, J., Löffler, M., Linke, O., Hartmann, M.,
1226 Herenz, P. and Stratmann, F.: Annual variability of ice-nucleating particle concentrations at different
1227 Arctic locations, *Atmos. Chem. Phys.*, 19(7), 5293–5311, doi:10.5194/acp-19-5293-2019, 2019.

1228 Whale, T. F., Murray, B. J., O’Sullivan, D., Wilson, T. W., Umo, N. S., Baustian, K. J., Atkinson, J. D.,
1229 Workneh, D. A. and Morris, G. J.: A technique for quantifying heterogeneous ice nucleation in microlitre
1230 supercooled water droplets, *Atmos. Meas. Tech.*, 8(6), 2437–2447, doi:10.5194/amt-8-2437-2015, 2015.

1231 Wilson, T. W., Ladino, L. a., Alpert, P. a., Breckels, M. N., Brooks, I. M., Browse, J., Burrows, S. M.,
1232 Carslaw, K. S., Huffman, J. A., Judd, C., Kilhau, W. P., Mason, R. H., McFiggans, G., Miller, L. a.,
1233 Nájera, J. J., Polishchuk, E., Rae, S., Schiller, C. L., Si, M., Temprado, J. V., Whale, T. F., Wong, J. P. S.,
1234 Wurl, O., Yakobi-Hancock, J. D., Abbatt, J. P. D., Aller, J. Y., Bertram, A. K., Knopf, D. a. and Murray,
1235 B. J.: A marine biogenic source of atmospheric ice-nucleating particles, *Nature*, 525(7568), 234–238,
1236 doi:10.1038/nature14986, 2015.

1237 Wu, W.-S., Purser, R. J. and Parrish, D. F.: Three-Dimensional Variational Analysis with Spatially
1238 Inhomogeneous Covariances, *Mon. Weather Rev.*, 130(12), 2905–2916, doi:10.1175/1520-
1239 0493(2002)130<2905:TDVAWS>2.0.CO;2, 2002.

1240 Yadav, S., Venezia, R. E., Paerl, R. W. and Petters, M. D.: Characterization of Ice-Nucleating Particles
1241 Over Northern India, *J. Geophys. Res. Atmos.*, 124(19), 10467–10482,
1242 doi:https://doi.org/10.1029/2019JD030702, 2019.

1243 Yahya, R. Z., Arrieta, J. M., Cusack, M. and Duarte, C. M.: Airborne Prokaryote and Virus Abundance
1244 Over the Red Sea, *Front. Microbiol.*, 10, 1112, doi:10.3389/fmicb.2019.01112, 2019.

- 1245 Yang, J., Wang, Z., Heymsfield, A. J., DeMott, P. J., Twohy, C. H., Suski, K. J. and Toohey, D. W.: High
1246 ice concentration observed in tropical maritime stratiform mixed-phase clouds with top temperatures
1247 warmer than -8°C , *Atmos. Res.*, 233, 104719, doi:<https://doi.org/10.1016/j.atmosres.2019.104719>, 2020.
- 1248 Yost, J. L. and Hartemink, A. E.: Chapter Four - Soil organic carbon in sandy soils: A review, vol. 158,
1249 edited by D. L. Sparks, pp. 217–310, Academic Press., 2019.
- 1250 Yu, Y., Kalashnikova, O. V, Garay, M. J., Lee, H. and Notaro, M.: Identification and Characterization of
1251 Dust Source Regions Across North Africa and the Middle East Using MISR Satellite Observations,
1252 *Geophys. Res. Lett.*, 45(13), 6690–6701, doi:<https://doi.org/10.1029/2018GL078324>, 2018.
- 1253 Zolles, T., Burkart, J., Häusler, T., Pummer, B., Hitzenberger, R. and Grothe, H.: Identification of Ice
1254 Nucleation Active Sites on Feldspar Dust Particles, *J. Phys. Chem. A*, 119(11), 2692–2700,
1255 doi:[10.1021/jp509839x](https://doi.org/10.1021/jp509839x), 2015.
- 1256